POLITECNICO DI TORINO

I Faculty of Engineering

Master of Science in Environmental Engineering

(Petroleum Engineering Program)

SIMULATION OF FLUID FLOW AND MICRO-FRACTURES IN SYINTHETIC SANDSTONE

Tutor (s):

Dr. Jan Ter Heege

Prof. Raffaele Romagnoli

Student: Rossi C. Mendez C.

March, 2012

ACKNOWLEDGEMENT

I would like to express my sincerest gratitude my supervisors in TNO and Polytechnic of Turin: Dr. Jan Ter Heege and Raffaele Romagnoli for their supervision and guidance from the very early stage of this thesis as well as providing me with his advice throughout the work.

This thesis would not have been possible without the support and insights of my professor, and supervisor Dr. Peter Fokker who has given his all out support, valuable experience, guidance and motivation on my thesis subject.

I wish to thank my entire family and my friends for their support, friendship and providing loving environment for me.

Lastly, and most importantly, my parents deserve special tribute for encouraging me, being supportive of my chosen path.

Utrecht, March 2012.

Rossi Mendez

ABSTRACT

Simulation of fracture patterns represents one of the big challenges in Geomechanics due to its complexity. Schematic representation of the shape and dimension of fractures are generally difficult to perform. Nowadays, there are several numerical model developed with the aim of modeling fracturing pressures and the resulting fracture geometries. However, most available models require the indication of fracture initiation and fracture propagation within the rock. Therefore, there is a limitation within the simulation that constrains the ability of the model for predicting fracture behavior.

The project thesis will discuss how to model hydraulic fracturing and fluid flow in synthetic sandstones at a specific state of stress. Discrete element models (PFC2D) are used to simulate these processes. Particle Flow Code or PFC2D is a discontinue code that simulates the interactions and movements between the discretized particles. The rock is treated as group of particles or disks that are moving in a specific region. The synthetic sample shows good agreement with typical petrophysical and mechanical values of real sandstones. Darcy flow and hydraulic fracturing were reproduced by setting a fluid flow network within the discretized model .The results exhibit a positive correlation with common behavior of rocks that are under the effect of a process like hydraulic fracturing.

LIST OF CONTENTS

LIST OF TABLES

LIST OF FIGURES

1 INTRODUCTION

The extraction of geothermal energy is generally performed by drilling an injection and production well into hot rock that are connected by a region of fractured rock. The purpose of this arrangement is to subtract pressurized hot water from the production well and inject water at surface temperature in the injection well. The fractured region which is the rock volume located between both wells is often created by injecting high pressure water (i.e. hydraulic fracturing). For optimizing fracturing techniques, study of fluid flow through fractured rock under the effect of different state of stress is essential.

It is important to obtain a detailed understanding of the initiation, propagation and reactivation of fractures in the hot rock when hydraulic fracturing is applied. The initiation of fractures occurs when the local concentration of stress in the rock overcomes the rock tensile strength. Propagation of the fractures after initiation depends on the effective stresses at the crack tip and rock properties. In case of existing fractures the magnitude of stress required for fracture reactivation is less than the strength of the rock, and dependent on fracture geometry, micro-structural state and friction coefficient.

Particle flow code (PFC^{2D}) is commercial software that is used for analysis, testing and research. Nowadays, there are many numerical simulators that are able to model hydraulic fracturing pressures and the resultant fractures geometries. However, most of the available numerical models require the specification of where the fracture will initiate and how it will propagate within the synthetic rock. The main advantage of using PFC^{2D} is based on the idea that those specifications are not required. The assembly will fail as soon as the applied stresses equal or exceed the mechanical strength of the sample and then, fracture patterns will develop within the bonded particle system. This study shows the initiation and further propagation of a fracture within synthetic sandstone when pressurized water is injected.

Modeling the development of fracture patterns represents one of the big challenges in geomechanics due to its complexity and importance in different fields (geomechanics, geothermal, geology, petroleum sciences etc.). Simulations that mimic the shape and dimension of fractures are generally difficult to perform. In the simplest approach, it is assumed that fractures are channels or parallel plates. However, it is clear that fractures do not resemble perfect channel geometry. Instead the fracture system is characterized by irregular paths with changing aperture along the fracture.

The aim of this study is to model hydraulic fracturing and fluid flow in sandstones at a specific state of stress. Discrete element models sandstones (PFC^{2D}) are used to simulate these processes. Sandstones are reproduced using the bonded particle model. The Bonded Particle Model (BPM) is a model in which the rock is discretized as an assembly of disks (2D) or spheres (3D). The disks or spheres are connected by inter-granular bonds and the micro-mechanical properties of the elements and bonds are selected to match the macroscopic mechanical behavior of the rock. The model can be extended to simulate fluid flow by defining fluid domains based on element arrangement.

Simulations with varying key parameters (material strength, material geometrical properties, insitu state of stress, injected pressures etc) determine fracture pattern development in the material. The variation in the development of fracture patterns under different deformation conditions and rock properties such as mechanical strength can be extracted from the model. The results are used to determine changes in mechanical and fluid flow properties of sandstones due to deformation at varying loading conditions and investigate typical fracture patterns.

2 THEORY AND BACKGROUND

2.1 **Modeling fluid flow & Mechanical Properties.**

2.1.1 Porosity & Permeability of Rock Materials

2.1.1.1 Intact Porous Rock

- **Kozeny- Carman Theory**

Hydraulic conductivity for single phase flow in intact porous rocks can be predicted by empirical relationships or theoretical models. By considering parameters like pore size, tortuosity and conductivity a correlation between permeability and porosity can be obtained. A relationship between permeability and properties of pores was presented by *Kozeny* (1927) and later modified by *Carman* (1938, 1956), known as Kozeny- Carman equation.

The Kozeny- Carman equation can be used to express permeability as a function of porosity (ø), specific surface (S), grain shape/pore shape and tortuosity (T). A common expression of Kozeny-Carman equation is *(Fjaer 2008:419):*

$$k = \frac{{d_g}^2}{K_o T^2} \frac{\emptyset^3}{(1-\emptyset^2)} \qquad (1)$$

Where d_g is defined as grain diameter (spherical shape), K_o is an empirical factor to account for realistic porous shape and T is the tortuosity of the capillary tube.

According to *Carrier III* (2003), the Kozeny- Carman formula has the following limitations:

-The formula is not appropriate for clay soils, because it assumes that there is no electrochemical reaction between soil particles and water.
- Kozeny- Carman is based on Darcian conditions which means laminar flow, low pore water velocity (Bernoulli energy term can be neglected), however as pore size increase and velocity increases, turbulent flow and inertia need to be considered.
- Varying pore structure with compaction is not considered, thus, the application of this equation is not appropriate in soil containing platy particles as mica.

- **Kozeny-Carman & Fractals Theory**

Kozeny-Carman equation is usually applied for permeability evaluation before drilling activities are performed. However, in many cases, the lack of petrophysical data and the assumption of constant grain size yield poorly constrained permeability predictions.

The main complication is to describe properly pore space in sedimentary rocks. Fractal theory can be applied to better describe pore space. The pore space of natural rocks is structured over a wide range of scales. This is exhibit by a fractal space model introduced by Pape (1982), the so called “Pigeon Hole” model. Based on this model, effective pore radius and permeability can be calculated assuming a multi-fractal structure. Due to the constrictions presented by capillaries, a differentiation between hydraulic radii reff and geometric pores rsite need to be done.

Figure 1 shows a representation of Pigeon Model. The geometrical pore sites are connected by hydraulic capillary channels of radius reff. The three radii rgrain, rsite and reff are the size parameters of the porous medium.

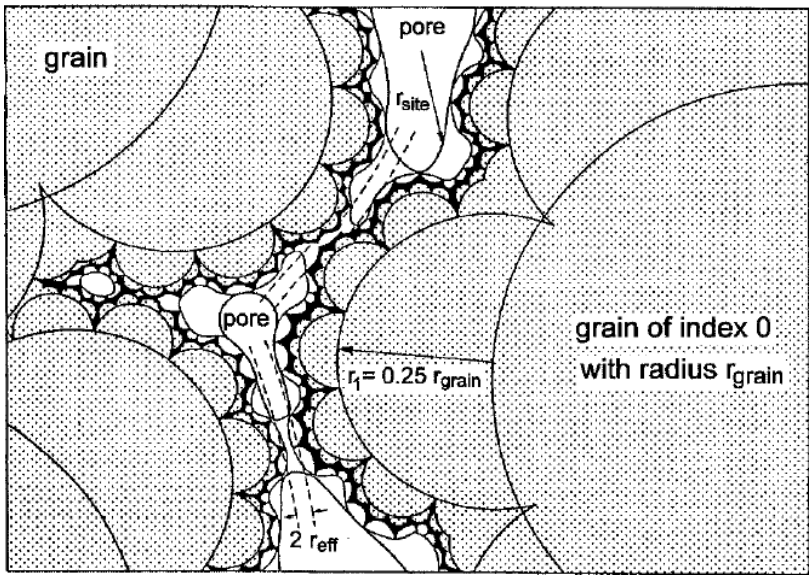

Fig.1: Cartoon showing a sedimentary rock according to the "pigeon hole" (Pape et al., 1987a) composed of geometrical pores with radius rsite and hydraulic capillaries with effective radius reff.

Where c1 corresponds to a fitting constant for sandstone when $^{r_{grain}}/_{r_{eff}} >$ 30.The typical value for sandstone is equal to 0.39 for the previous condition.

$$^{r_{grain}}/_{r_{site}} = \left(^{r_{grain}}/_{r_{eff}}\right)^{c1} \quad (1a)$$

This value has been obtained by an analysis of a large data set of sandstone (Hansgeorg Pape, 2000). Fractal theory can is based on the observation that the shape of the inner surface of rock pores follows a self-similar rule (the geometrical shape of the pore system under study can be split into parts, each of which is a reduced-size copy of the whole system). A combination of Kozeny-Carman equation and fractal theory (Pape, 1998) can be applied in order to get permeability values which better describe the real geometry of porous medium.

$$k = \frac{{r_{eff}}^2}{8F} \quad (2)$$

The previous formula gives permeability as a function of effective pore radius r_{eff} and formation resistivity factor F. Formation resistivity factor is considered to be directly proportional to porosity and inversely proportional to sample tortuosity.

$$F = \frac{\emptyset}{T} \tag{3}$$

Pape (1987a) represented tortuosity as a parameter that depends on pore radius and the effective radius of capillaries inside the hydraulic model. The main assumption relies on the fractal dimension (D) that characterizes the sample. Fractal dimension is defined according to the type of lithology under study, and it can vary from two to three ($2 < D < 3$). Figure 1 contains experimental data from Wenlu Zhu and Teng-Fong Wong (1997), parameters as grain size, porosity, permeability and Nur percolation factor (it is defined as the percentage of porous within a porous system that is not connected , it is known as non-effective or non-interconnected porosity) where used in order to evaluate the behavior of Kozeny-Carman equation. A comparison between the original Kozeny-Carman equation where particle radius is considered constant and the Kozeny-Carman equation by using fractal approach are implemented for permeability calculation upon intact porous rock.

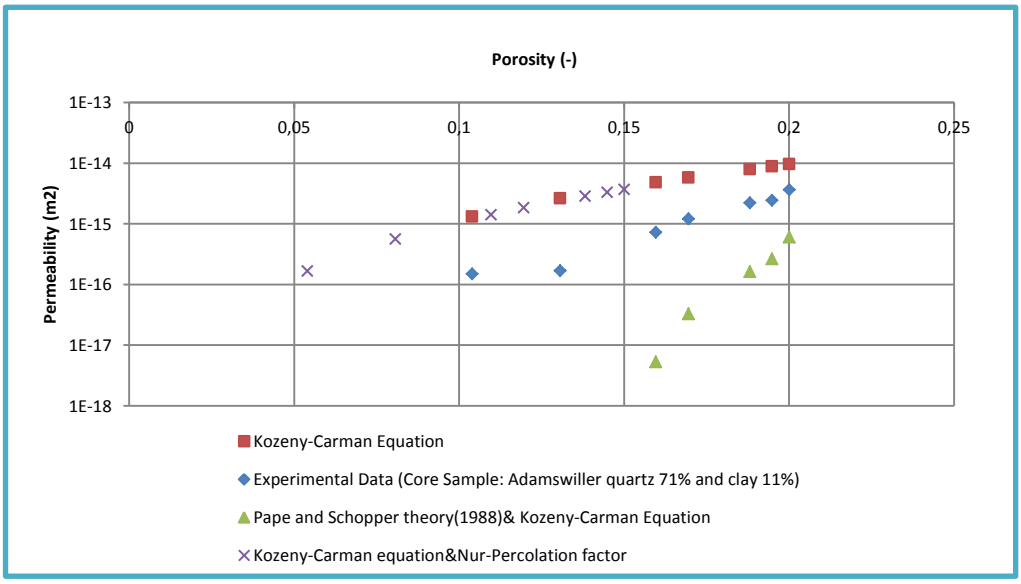

Fig.1a: Application of Kozeny-Carman equation by considering two geometrical approaches: constant grain size and Pape's fractal model.

The experimental data shows a better matching with Kozeny-Carman equation in which pore size is considered constant than with the fractal model of Pape (1998). Pape's equation has a higher degree of uncertainty and longer deviations from experimental data. The main reason for deviation can be explained in terms of fractal dimension (D). Kozeny-Carman equation and fractal theory generate an exponential equation whose exponent is a function of D, therefore any change in the exponent value will produce a large variation in permeability results. The level of dispersion in the results is considered to be due to the following:

- Presence of clay, which is a key factor in permeability estimation, but not considered inside Kozeny-Carman formula.
- Fractal dimension (D) is considered for typical sandstones equal to 2.36. However, this value can be different for different sandstones.
- Also tortuosity values are dependent of fractal dimension.

2.1.1.2 Fractured Rock Material

- **Parallel Plate Model**

The parallel plate model is a simple and common applied method (*Huitt* 1955; *Snow* 1965) for calculating fluid flow through a fractured rock. It is derived by assuming that fractures can be represented by two smooth parallel plates, separated by an aperture h. The cross-sectional area is considered as the effective area which fluid flows from inlet to outlet at a constant static pressure. It is assumed that the flow space is bounded by impermeable and rigid fracture walls (no- slip boundary condition) elsewhere.

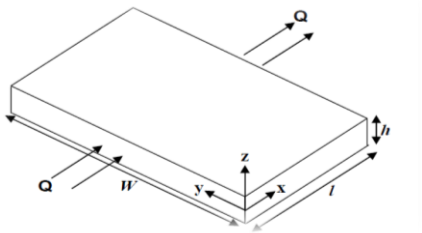

Fig. 2: Fluid Flow Modeling in Fractures. Sudipta Karsar, M.Nafi Toksoz (1989).

Wilkes (1999) proposed an analytical solution for pressure along the platens:

$$P(x) = P_i - \frac{x}{l}(P_i - P_o) \quad (4)$$

x = is the distance between the inlet pressure point and a second random point of pressure located along the platens in the x-direction.
l = is the distance between the inlet and outlet position (fracture length).
P_i = Inlet pressure
P_o = Outlet pressure
W= Fracture width

The system creates a uniform pressure gradient in the plane of the fracture, resulting in a unidirectional laminar flow through the system. For this case, only flow in the x-direction is considered. Therefore the x-component velocity u can be calculated by integrating the next equation from over the gap between the parallel plates.

$$u(z) = \frac{1}{2\mu}\left(\frac{P_i - P_o}{l}\right) z(h - z) \quad (5)$$

The total volumetric flux (Q_x) through the fracture is represented as:

$$Q_x = W \int_0^h u(z)dz \quad (6)$$

$$Q_x = W \int_0^h \frac{1}{2\mu}\left(\frac{P_i - P_o}{l}\right) z(h - z)dz \quad (7)$$

$$Q_x = W \frac{1}{2\mu}\left(\frac{P_i - P_o}{l}\right) \int_0^h z(h - z)dz \quad (8)$$

For a matter of simplification A will be equal to $\frac{1}{2\mu}\left(\frac{P_i - P_o}{l}\right) W$

$$Q_x = A\left[\frac{h^3}{2} - \frac{h^3}{3}\right] \tag{9}$$

$$Q_x = W\frac{h^3}{12\mu}\left(\frac{P_i - P_o}{l}\right) \tag{10}$$

The average velocity *u'* is calculated by dividing the total volumetric flux by the cross-sectional area, width (W) and height (h):

$$u' = \frac{Q_x}{Wh} = -\frac{h^2}{12\mu}\left(\frac{P_i - P_o}{l}\right) \tag{11}$$

Flow through porous media is written by using Darcy's Law, where dynamic viscosity μ and A cross-sectional area are represented in equation 12:

$$Q = -\frac{KA}{\mu}\left(\frac{P_i - P_o}{l}\right) \tag{12}$$

From the equation 10 and 12, the permeability of the fracture is as a function of the sample height:

$$k = \frac{h^2}{12} \tag{13}$$

Transmissivity is expressed as the product of permeability and cross-sectional area, yielding a cubic dependence of h^3 on transmissivity, hence, the origin of the name cubic law.

$$T = kA = {Wh^3}/{12} \tag{14}$$

In reality, fractures are not parallel plates but are two dimensional networks of variable aperture. According to *Tsang and Tsang* (1989), the fluid flow in single fractures

may not follow the cubic law. More complex model, including surface roughness factors should be considered for more realistic descriptions of fluid flow through fractures.

2.2 **Mechanical characterization of the rock.**

2.2.1 Mohr Coulomb Criterion

Mohr-Coulomb criterion assumes that shear failure occurs when the shear stress along a plane exceeds the friction strength. The failure is described as a function of the normal stresses applied to the material:

$$|\tau| = f(\sigma_n) \tag{15}$$

This criterion consists in a linear function $\boldsymbol{f}$ for shear failure characterization.The equation includes the inherent shear strength or cohesion c of the material, the coefficient of internal friction μ and the normal force on the body σ_n.

$$\tau = c + \mu\sigma_n \tag{16}$$

Figure 3 is a schematic representation of Mohr-Coulomb failure criterion. The use of Mohr's circle allows to determine which principal stresses (maximum principal stress σ_1 and minimum principal stress σ_3) will produce this combination of shear and normal stress (linear failure envelope), and the angle of the plane in which failure will occur.

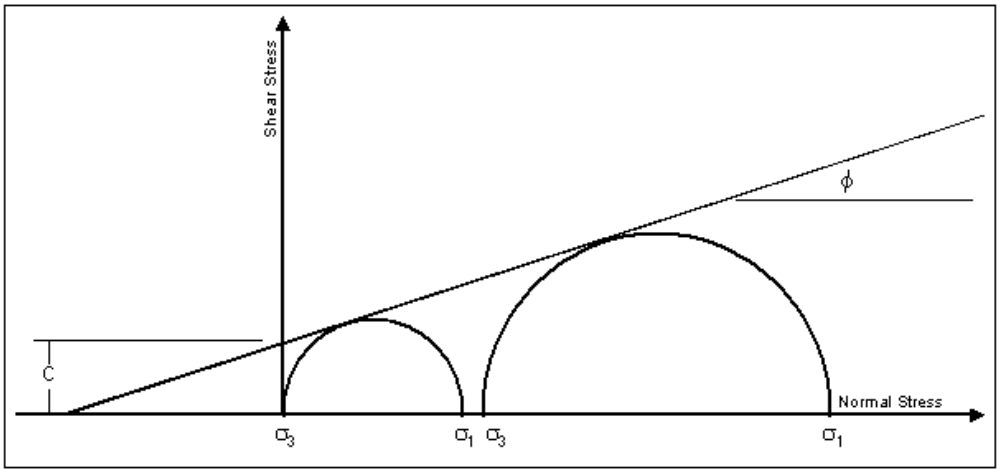

Fig. 3: *Mohr-Coulomb* criterion in τ- σ_n space.

The failure angle φ is associated to the internal friction by the following equation**:**

$$\mu = \tan(\varphi) \tag{17}$$

Many analyses related to the mechanical characterization of sandstones have pointed out that friction angle (φ) for sandstones should be around 30 degrees. However, these values can change from 10 degrees (soft rock) to 50 degrees (hard rock).

2.2.2 Hoek and Brown Criterion

In many rock materials, failure is observed to deviate from a linear failure criterion. In such case, the Hoek and Brown (1980) criterion may better describe rock strength. This failure approach is described by the following equation:

$$\sigma_1 = \sigma_3 + \sqrt{mC_0\sigma_3 + s\sigma_c{}^2} \tag{18}$$

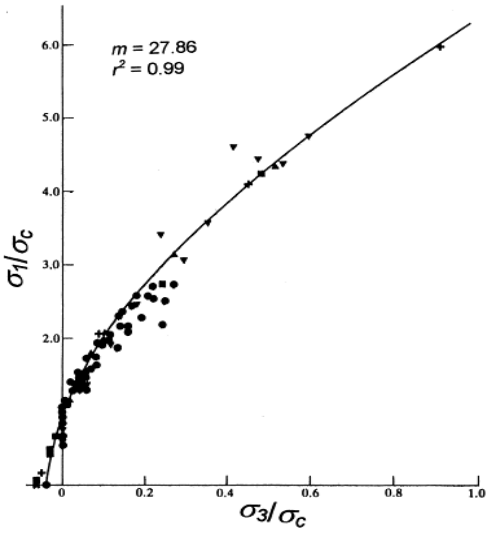

Fig. 4: *Hoek-Brown* criterion in $\sigma_1/\sigma_c - \sigma_3/\sigma_c$ plane.

Where σ_1 and σ_3 are the major and minor principal stresses at failure *Co* is the uniaxial compressive strength of the intact rock. The constant m is an empirical curve-fitting parameter and *S* is a constant related to the damage in the rocks usually takes values from 0,5 for fractured material or a value equal to 1 for intact rock mass. The uniaxial compressive strength of the fractured rock is defined as:

$$C_{of} = \sqrt{s\sigma_c{}^2} \tag{19}$$

This value(C_{of}) indicates the degree of damage in the sample.

Other failure criteria has been defined for predicting the conditions under which solid materials fail under the action of external loads. However, the study was restricted to Mohr-Coulomb and Hoek and Brown failure criteria. Others criterion are outside of the scope of study.

2.3 **Particle Flow Code (PFC2D)**

Particle Flow Code (Itasca) is a commercial software package that simulates the mechanical behavior of a material comprised of arbitrary circles (2D) or spheres (3D) particles (i.e. distinct element method-DEM).

The model is made of distinct elements, either circular or spherical elements, particles that are physically bonded together (cluster) or rigid bodies created by a set of overlapping particles (clumps) and contacts. It is particularly suitable for simulating brittle deformation within a material due to external or internal forces acting upon the particles. DEM was introduced by *Cundall* (1971) for the analysis of rock mechanics problems and then applied to soils by *Cundall and Strack* (1979). PFC^{2D} is a simplified Distinct Element Model (i.e. it is classified as simplified because DEM is able to handle polygonal shapes and PFC2D only circular rigid bodies are considered).

The model contains the main assumptions (Itasca Manual, 2006):

1. The particles act as rigid bodies.
2. The contacts occur over vanishingly small area.
3. Behavior at the contact uses a soft-contact approach, where the rigid particles are allowed to overlap one another at contact points to model elastic deformation.
4. The magnitude of the contact force is related to element overlap and contact stiffness by using force-displacement laws.
5. Parallel bonds and contact bonds can exist at contact between particles.

The force displacement law is applied at each contact point and it relates the particles displacement and the forces that originate particle motion at a specific point of contact. During simulation two approaches are combined, law of motion and force-displacement law. The equations are applied at each particle inside the assembly and each contact between balls. This approach is efficient to determine the mechanical behavior of a compacted granular assembly, as deformation is the product of sliding and rotation of rigid bodies. The motion law is applied in order to obtain the displacement of each particle due to contacts and body forces acting upon it. The force-displacement law is used to update contact forces produced at contact point due to particles movement and overlap.

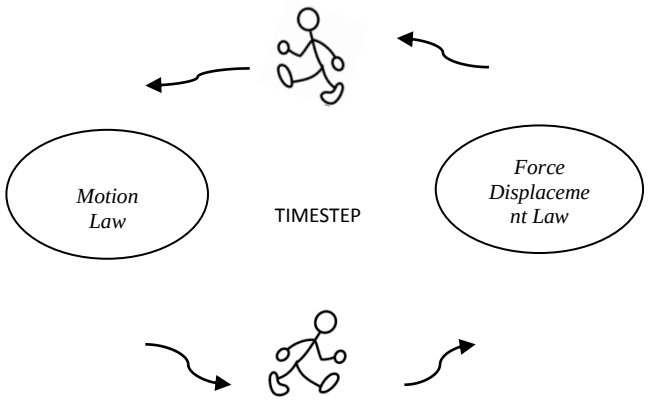

Fig.5: PFC2D internal dynamics at each time step.

The contacts inside of the assembly can be given cohesive strength by applying either contact bonds or parallel bonds. A Contact bond can be interpreted as a point of contact that keeps together the contacting entities and transmits the force acting upon the contact. Tensile and shear contact strength are the two parameters that allow to define contact bonds. The bond will break when either the tensile force applied to the contact overcomes the established bond tensile strength or the shear contact force exceeds the bond shear contact strength.

Parallel bonds can be seen as a cementing element between particles (disks). This type of bond presents a circular or a rectangular area that is able to transmit forces and moments. The parallel bond normal stiffness (stress/displacement), parallel bond shear stiffness (stress/displacement), shear strength (force), normal strength (units of force) and bond radius are the parameters that define the existence of parallel bond within the model.

The analysis is done between the two contacting entities which can be ball-ball or ball-wall (wall is understood as a specific boundary defined within model before simulation in order to confine the space where the particles are generated). The calculations are referred to the interception point $Xi^{[C]}$, which lies on a contact plane.

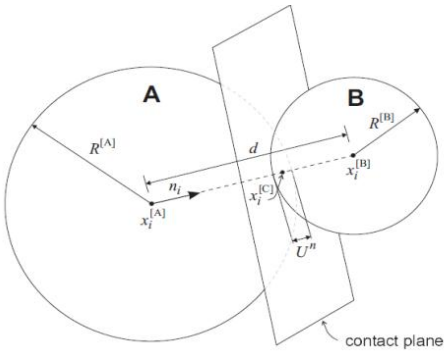

Fig.6: Schematization of a ball-ball contact, Itasca Manual (2006).

The contact force vector is split into normal and shear component with respect to the contact plane located at the interception point $Xi^{[C]}$. Shear and normal force magnitude are a function of shear and normal stiffness of the contact and shear and normal displacement.

$$F_i = {F_i}^n + {F_i}^s \tag{20}$$

Shear and tensile forces are set to zero at the starting point of the simulations. The shear and contact force are formed by summing shear and normal force that develop during each time step.

$$F^n = {F_i}^n + \Delta {F_i}^n \tag{21}$$

$$F^s = F^s + \Delta {F_i}^s \tag{22}$$

Thus, the resultant force and moment acting on the two entities in contact, which are denoted as $\emptyset_1$ and $\emptyset_2$, is calculated (if the bond does not break) by considering the sum of all forces $\sum F$ and moments $\sum M_3$ affecting each element in contact within the model.

$${F_i}^{[\emptyset_1]} \leftarrow {F_i}^{[\emptyset_1]} - F_i \tag{23}$$

$${F_i}^{[\emptyset_2]} \leftarrow {F_i}^{[\emptyset_2]} - F_i \tag{24}$$

$${M_3}^{[\emptyset_1]} \leftarrow {M_3}^{[\emptyset_1]} - e_{3jk}\left({x_j}^{[C]} - {x_j}^{[\emptyset_1]}\right)F_k \tag{25}$$

$${M_3}^{[\emptyset_2]} \leftarrow {M_3}^{[\emptyset_2]} - e_{3jk}\left({x_j}^{[C]} - {x_j}^{[\emptyset_2]}\right)F_k \tag{26}$$

A similar scenario is considered when parallel bonds are set inside the granular assembly. The approach is analogous to that described for contact bond model, however, the difference between both model lies on the idea that total force and moment associated with each particle in contact will be affected by the presence of a circular or rectangular bond between the contacting entities (ball A and ball B), while for contact bond model the equation are related to a point.

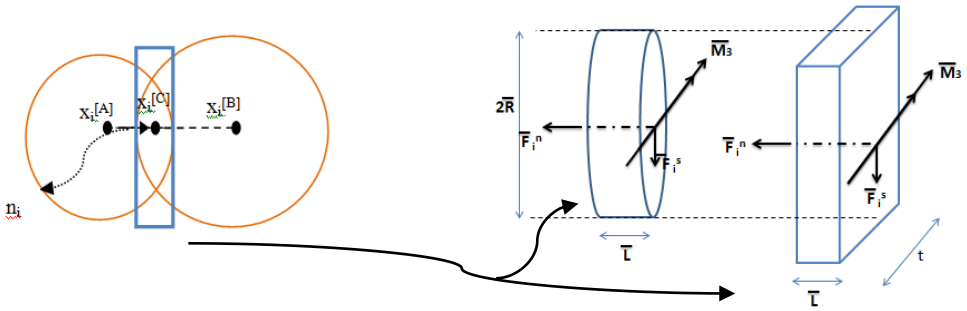

Fig.7: Parallel Bond Idealization, Itasca Manual (2006).

The calculation of the force-displacement law applied to one contact can be summarized as follows. Knowing the position of the contacting entities (i.e. the centroid of two random balls A and B with geometric centers defined as $Xi^{[A]}$ and $Xi^{[B]}$), balls radius ($R^{[A]}$ and $R^{[b]}$), particle normal displacement U^n and the vector n_i normal to the contacting plane, calculation of the contacting point between both elements is performed. When the contact is between two balls equation 27 is used however, in case tha the contacting entities are ball-wall equation 28 is applied.

$$x^{[C]}{}_i = x_i{}^{[A]} + \left(R^{[A]} - \frac{1}{2}U^n\right)n_i \tag{27}$$

$$x^{[C]}{}_i = x_i{}^{[b]} + \left(R^{[b]} - \frac{1}{2}U^n\right)n_i \tag{28}$$

The translational velocity and rotational velocity of each element is defined at every step of the simulation. The positions of the particles are updated and then, particles velocities and accelerations are computed. Calculation of translational velocities involve parameters as, total mass of the disk m, contact force vector F_i, body force acceleration vector g and the defined calculation cycle Δt. By inserting equation 34 and equation 35 into equation 28 and 29 velocities are calculated as following:

$$\dot{x}_i{}^{\left(t+\frac{\Delta t}{2}\right)} = \dot{x}_i{}^{\left(t-\frac{\Delta t}{2}\right)} + \left(\frac{F_i{}^{(t)}}{m} + g_i\right)\Delta t \tag{29}$$

$$w_3^{\left(t+\frac{\Delta t}{2}\right)} = w_3^{\left(t-\frac{\Delta t}{2}\right)} + \left(\frac{M_3^{(t)}}{I}\right)\Delta t \quad (30)$$

$$\ddot{x}_\iota^{(t)} = \frac{1}{\Delta t}\left(\dot{x}_\iota^{(t+\frac{\Delta t}{2})} - \dot{x}_i^{(t-\Delta t/2)}\right) \quad (31)$$

$$\dot{w}_3^{(t)} = \frac{1}{\Delta t}\left(w_3^{(t+\frac{\Delta t}{2})} - w_3^{(t-\Delta t/2)}\right) \quad (32)$$

The normal displacement $U_i^n$and shear displacement ΔU_i^s are calculated on the basis of balls dimension, geometric center position and time step used for simulating the model. Equation 33 (in case of ball-ball contact) and Equation 34 (in case of ball-wall contact) are applied in order to estimate particle normal displacement. The distance between the centroid of both contacting entities is defined as d.

$$U^n = R^{[A]} + R^{[B]} - d \quad (33)$$

$$U^n = R^{[b]} - d \quad (34)$$

Normal displacement U_i^n is defined by considering ball geometry $R_i^{[A,B]}$, and centroid position. The shear displacement ΔU_i^s is estimated by calculating the relative shear velocity of ball A with respect to ball B.

$$\Delta U^s = V^s \Delta t \quad (35)$$

Where shear velocity V^s is obtained by applying equation 36 that is a function of contacting particles translational and rotational velocity, position of the contacting point and location of particles geometrical centers.

$$V^s = \left(\dot{x}_\iota^{[\emptyset^2]} - \dot{x}_\iota^{[\emptyset^1]}\right) t_i - w_3^{[\emptyset^2]}\left|x_k^{[C]} - x_k^{[\emptyset^2]}\right| - w_3^{[\emptyset^1]}\left|x_k^{[C]} - x_k^{[\emptyset^1]}\right| \quad (36)$$

Once the normal U^n and shear displacement $\Delta U^s$are known and the stiffness coefficients (normal and shear stiffness coefficients) at contact are set within the model, contacts force magnitudes are estimated.

$$\Delta F^S = -k^s \Delta U_s \tag{37}$$

$$F^n = K^n U^n \tag{38}$$

If the contacts do not break during simulations, a calculation of total force and moments acting upon the contacts is performed. Table 1 shows the equations within the force-displacement cycle for contact bond model and parallel bond model.

	CONTACT BOND MODEL	PARALLEL BOND MODEL
	Ball-Ball Contact/ Ball-Wall Contact	Ball-Ball Contact
Contact Force Vector	$F_i = {F_i}^n + {F_i}^s$	$\bar{F}_i = {\bar{F}_i}^n + {\bar{F}_i}^s$
Normal Force Magnitude	$F^n = K^n U^n$	${\bar{F}_i}^n = \bar{k}^n A \Delta {U_i}^n n_i$
Shear Force Magnitude	$\Delta F^S = -k^s \Delta U_s$	$\Delta \bar{F}^S = -\bar{k}^s A \Delta {U_i}^S$
Resultant Force in entity 1	${F_i}^{[\emptyset_1]} \leftarrow {F_i}^{[\emptyset_1]} - F_i$	${\bar{F}_i}^{[A]} \leftarrow {\bar{F}_i}^{[A]} - \bar{F}_i$
Resultant Force in entity 2	${F_i}^{[\emptyset_2]} \leftarrow {F_i}^{[\emptyset_2]} - F_i$	${\bar{F}_i}^{[B]} \leftarrow {\bar{F}_i}^{[B]} - \bar{F}_i$
Resultant Moment in entity 1	${M_3}^{[\emptyset_1]} \leftarrow {M_3}^{[\emptyset_1]} - e_{3jk}({x_j}^{[C]} - {x_j}^{[\emptyset_1]})F_k$	${M_3}^{[A]} \leftarrow {M_3}^{[A]} - e_{3jk}({x_j}^{[C]} - {x_j}^{[A]})F_k$
Resultant Moment in entity 2	${M_3}^{[\emptyset_2]} \leftarrow {M_3}^{[\emptyset_2]} - e_{3jk}({x_j}^{[C]} - {x_j}^{[\emptyset_2]})F_k$	${M_3}^{[B]} \leftarrow {M_3}^{[B]} - e_{3jk}({x_j}^{[C]} - {x_j}^{[B]})F_k$

Table.1: Equations applied for estimating Moments and Forces acting upon the particle during Force-Displacement cycle.

While the force-displacement law is applied to the assembly, in parallel the movements of single granular elements are calculated by the resultant force and moment vectors acting upon the entity. The translational motion of each particle is calculated by considering parameters as: forces acting on the body F_i , total mass of the particle *m*, body force acceleration vector g and particle acceleration $\ddot{x}_i$ .The translational motion is calculated by applying equation 39:

$$F_i = m(\ddot{x}_\iota - g_i) \tag{39}$$

The rotational motion of the particles and the angular momentum of the particle H_i are related and the resultant moment acting upon the particle M_i is established.

Rotational Motion: $M_i = \dot{H}_i$

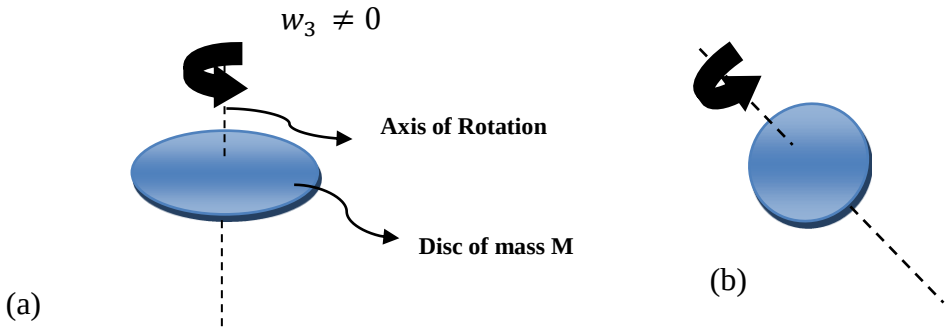

Fig.8: Moment of Inertia (a) Disk and (b) sphere.

The previous relation is referred to a local coordinate system located at the center of mass of the particle. For simplification, the local coordinate system of the particle is considered to be oriented along the principal axes of inertia of the entity (disk 2D or ball 3D) and thus, the moments of inertia in the main axes become equal to one another.

Therefore, the resultant moments of inertia related to the principal axes, I_1, I_2 and I_3 and angular accelerations about principal axes $\dot{w}_1$, $\dot{w}_2$ and $\dot{w}_3$ are simplified and expressed by the equation 43.

$$M_1 = I_1\dot{w}_1 + (I_3 - I_2)w_3w_2 \tag{40}$$

$$M_2 = I_2\dot{w}_2 + (I_1 - I_3)w_1w_3 \tag{41}$$

$$M_3 = I_3\dot{w}_3 + (I_2 - I_1)w_2w_1 \tag{42}$$

$$M_3 = I\dot{w}_3 = (\beta mR^2)\dot{w}_3 \tag{43}$$

As a final result the rotational motion of a particle (ball or disk) is a function of angular velocity and moment of inertia of the particle.

3 SIMULATION OF BONDED PARTICLE MODEL

Mechanical behavior analysis of a real rock under different state of stress is a challenging task of study. Nowadays with the increase of processor performance, detailed simulation of structures like sandstones can be reproduced with a high level of accuracy.

3.1 Calibration of compacted model.

In order to simulate synthetic sandstone whose mechanical properties resemble those of a real rock, a calibration process is performed. After, the micro-mechanical model (model created on the basis of micro-physical parameters such as, particle radius, bond stiffness, normal bond strength, shear bond strength, particle friction coefficient, etc.) is generated, the next step entails that the micro-properties simulated in the model correspond to the properties obtained from experimental data (Young's Modulus, Poisson ratio, friction coefficient, shear strength and others).

The process consists in subjecting the bonded particle model (BPM) to confining pressures and axial stresses. The idea is to perform a series of compression tests upon the assembly in an attempt to adjust the micro-mechanical properties of the model. The result should be a model whose mechanical characteristics resemble the macro-mechanical properties obtained from laboratory test. This process is repeated until the simulated micro-properties catch the required macro-mechanical properties. Once the micro-model reproduces the required real macro-properties, the model is considered to be calibrated.

Parameters like particle radius, contact stiffness ratio, particle stiffness, particle friction coefficient and others constitute the micro-mechanical model. The values used for this model in the first trial are selected according to typical values of the structure that is going to be simulated. Tuning of those values is performed by checking the calibration file generated during simulation. These values (micro-parameters) are adjusted according to the results obtained from the simulation.

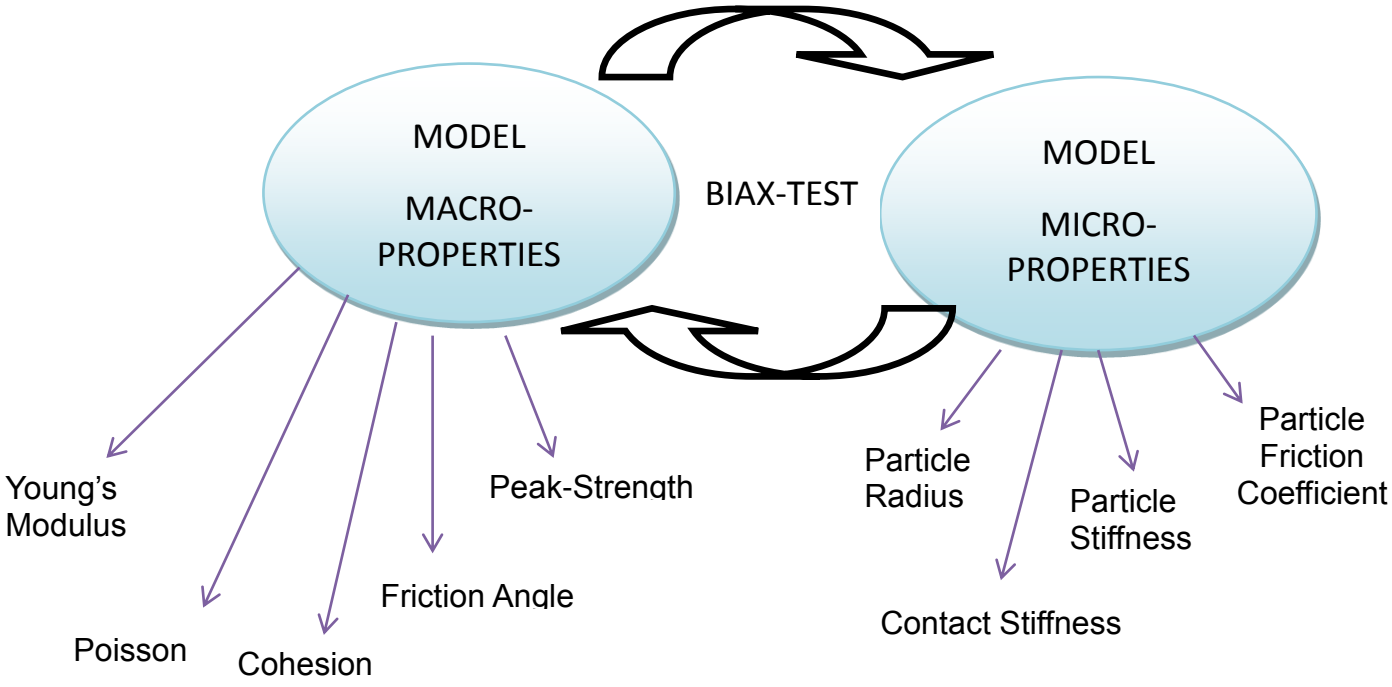

Fig.9: Calibration Process inside PFC^{2D}.

Once the micro-parameters that generate the proper values of Young's modulus, Poisson ratio and peak strength are introduced in the final micro-mechanical model the sample go through a failure criterion analysis. Mohr Coulomb criterion is used in order to estimate cohesion and internal friction coefficient of the sample under different axial and confined state of stress.

3.2 Fluid Flow Modeling and mechanical coupling through synthetic sandstone.

Fluid flow modeling of a compacted bonded assembly of particles is generated by designing a fluid flow network within the model. This study considers synthetic sandstone of low porosity .Therefore, the contribution of the matrix is neglected. The flow pathways reflect to be made of parallel–plate channels at their particle contacts. They are interpreted within the model as pipes or tubes where fluid flows. To determine the fluid network within the model, an important element calls domain needs to be defined within the network.

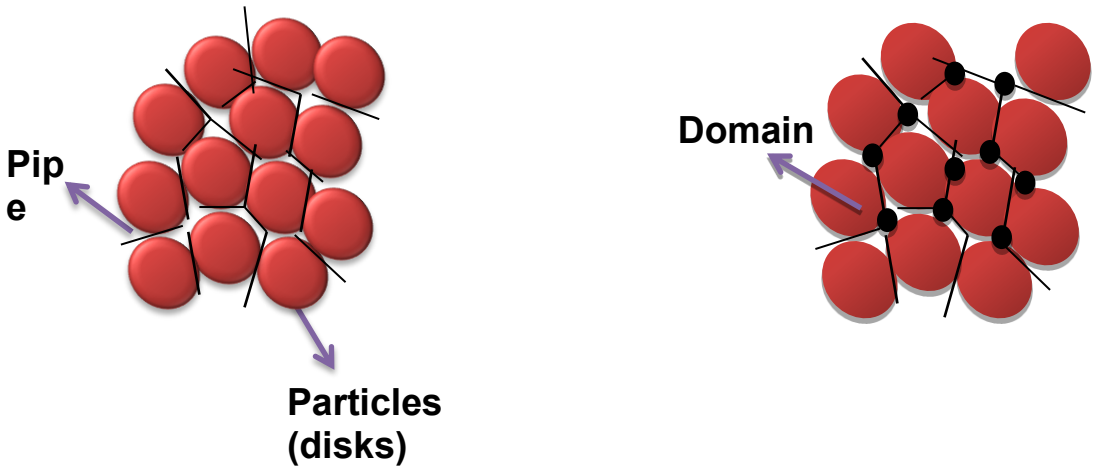

Fig.10: Bonded Particle Model and flow path (left). Domains, bonded particles and flow path (right).

A domain is defined inside the model as a closed chain of particles, whose volume depends on the volume of the surrounding pipes. These domains are connected to each pipe and thus, they storage and transmit any change in pressure within the fluid network during simulations. Figure 12 represents the center of the domains whiles the black lines between centers are the flow paths or pipes.

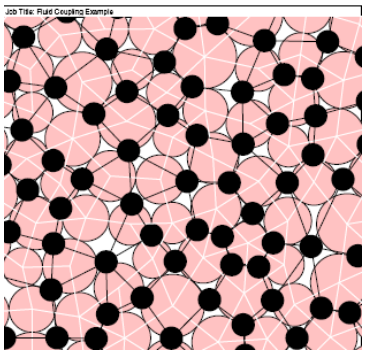

Fig.11: Particle Bonded Model and Fluid Flow Network, Itasca Manual 2006.

The link between domains is considered a point of crack, in case the normal or shear force applied to the contact overcome either the normal or shear strength of the contact bond. The flow through the pipe is calculated during simulation by using the following equation:

$$q = ka^3 \frac{(P_2 - P_1)}{L} \tag{44}$$

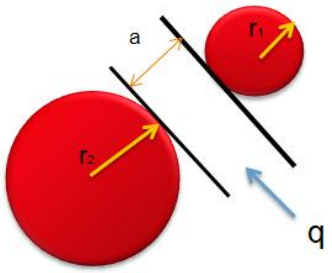

Fig.12: **Idealized fluid flow between two elements (disks).**

The flow rate through each pipe is defined as *q*, pipe length is L (inside the model L is calculated by considering an average diameter of the particles), $(P_2 - P_1)$ represents the pressure difference between the two adjacent domains and finally fracture aperture defined as *a*. The fracture aperture *a* is determined by the following equation:

$$a = \frac{a_0 F_0}{F + F_0} \tag{45}$$

Where F_o represents the value of the contact normal compressive force applied to the contact, F is the required contact normal compressive force to decrease the sample aperture up to half of the initial value. However, for this study the fracture aperture is considered to be constant, thus the normal force F required to decrease the hydraulic aperture (a) is set above the values established for the contact forces that may develop inside the system in order to guarantee that no change in aperture will be produced.

In case the normal force acting within the system is pure tensile, the aperture or gap between two entities in contact (a) is calculated by taking into account the residual aperture and adding the actual distance located at the two balls which is scaled by using a dimensionless multiplier m.

$$a = a_0 + mg \tag{46}$$

The change in pressure within the domains is based on the idea of an exchange of fluids between domains. The parameters that influence the fluid flow between particles are two: k_f fluid bulk modulus and V_d apparent volume of the domain.

$$\Delta P = \frac{k_f}{V_d}\left(\sum q\Delta t - \Delta V_d\right) \tag{47}$$

The mechanical coupling between fluid and bonded solid particles can be achieved by changing contact forces. The variations in contact forces originate opening or closing of contacts and therefore a change in fracture aperture. As a consequence of changing fracture aperture, the flow resistance to flow can be increased or decreased inside the model. Another way of mechanical coupling is reached by changing the domain volume. This change in volume produces an alteration in domain pressures. Traction exerted by domain pressures on enclosing particle is the last form of coupling usually used (Itasca Manual 2006).

3.3 Hydraulic fracturing simulation through synthetic sandstone.

The last part of the simulation is focused on generating the hydraulic fracturing conditions by injecting 1 MPa of pressure at the center of the assembly. Table 2 demonstrates the properties of the particles and fluid conditions needed for the simulation.

The applied procedure is similar to the one used during the fluid flow, however, in this case the domains will receive a pressure difference in a localized position of the fluid flow network.

SRM PROPERTIES	International System Units (SI)
Normal Force (F_O)	$5x10^5$
Multiplier Factor (m)	0.2
Water Bulk Modulus (bulk_w)	2.2e9
Dynvisc_w	5.0e-4

Table.2: Hydraulic Fracturing conditions within SRM.

Prior to injection, an anisotropic state of stress is generated within the bonded particle by displacement of upper and lower boundaries. The resulting assembly presents a vertical stress higher than the stress obtained in the horizontal direction.

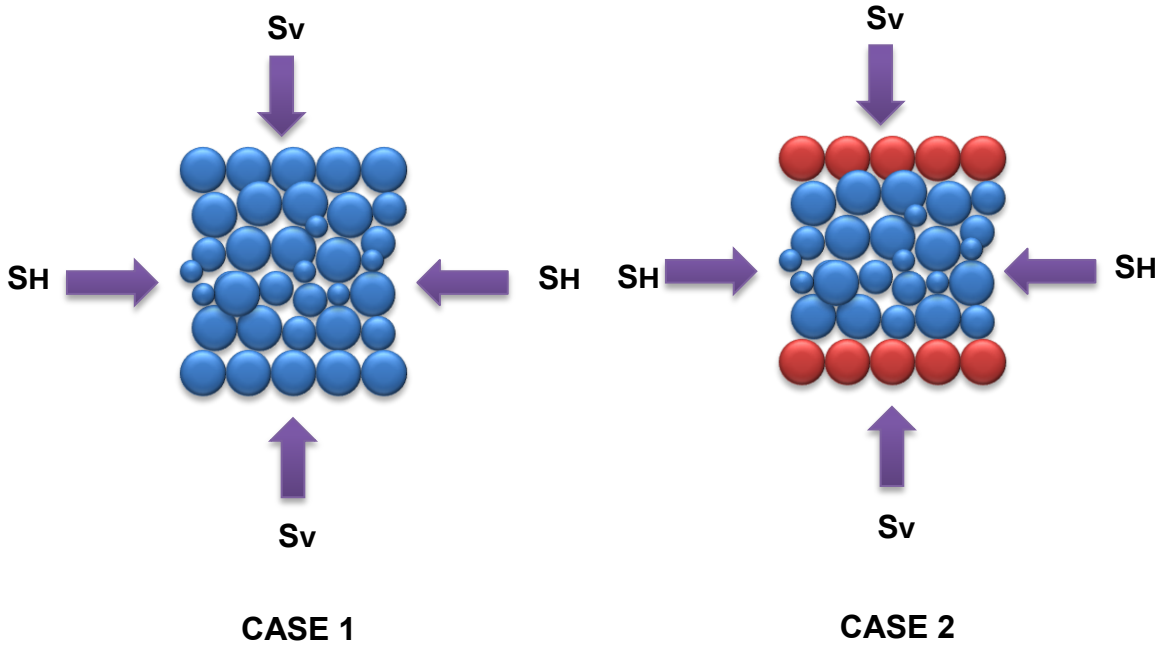

Fig.13: **BPM at isotropic state of stress S_H = Sv (Case1) and BPM at anisotropic state of stress S_H > Sv (Case 2).**

Within the model, there are compressive forces and tensile forces. The compressive force produces the largest force within the model due to the established initial conditions. The injected pressure is represented as a set of circles. The dimension of those circles depends on the amount of pressure injected. In order to reproduce the hydraulic fracturing process the strength of the contact between disks needs to be overcome.

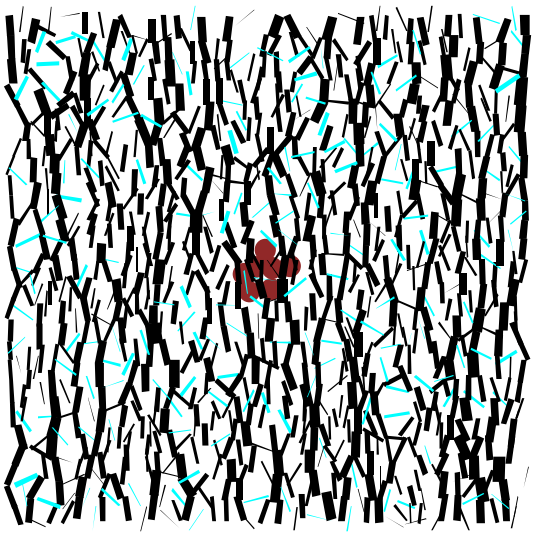

Fig.14: **Compressive forces (black lines), tensile forces (blue lines) and injected pressure (brown circles).**

4 SIMULATION RESULTS AND DISCUSSIONS

The synthetic model simulation implemented for rock mass mechanical characterization was generated by Particle Flow Code 2D, Itasca. Inside PFC^{2D} the rock is taken as a group of rigid particles of non-uniform sized that are bonded together at their contact points. This model is known as Bonded Particle Model and so far it has been performed by PFC^{2D} in which the grains are simulated as rounded disks.

4.1 Calibration results

Hard sandstone of low porosity has been selected for the development of this study, by applying the proposed calibration procedure. The corresponding micro-parameters of the simulated bonded particle model are obtained in order to fit the mechanical response of the synthetic rock mass at macro-scale. The macro-properties of the synthetic sandstones are given in Table 3.

MACRO-PROPERTIES	SI
Young's Modulus (**E**)	3,42E9E9
Poisson Ratio (**v**)	0.242
Uniaxial Compressive Strength ($\boldsymbol{\sigma_c}$)	-24.1E6
Material Cohesion (**c**)	3,347E5
Friction Angle (ϕ)	26,05º

Table.3: **Macro-properties of synthetic rock mass (SRM).**

Table 4 introduces the resultant micro-properties obtained from a calibration process applied to SRM. The introduced macro-properties are simulated by setting the following micro-properties in PFC^{2D}. The location of the centroid and the dimension of interacting particles are one of the main parameters necessary for establishing the system.

The selected dimension for the model (36 m x 36 m) was done in order to represent the mechanical behavior and the initial properties of a reservoir.

MODEL CHARACTERISTICS	SI
Model Width	36.0
Model Height	36.0
ELEMENT PROPERTIES	
Minimum Element Radius	0.35
Ratio Radius	1.66
Element Density	2649.0
Element Thickness	1.0
Element Friction	0.28
CONTACT PROPERTIES	
Contact Young's Modulus (**Ec**)	5.0E9
Mean Contact Bond Strength(normal)	1.0E6
Mean Contact Bond Strength (shear)	1.0E6

Table.4: Simulated Synthetic Rock Mass (SRM).

The results obtained from the mentioned calibration process carried out over the synthetic sandstone, by which material grains are simulated as random-shaped particles, show good agreement with the mechanical and physical properties of real sandstone. This calibration is based on the results of standard compressive test, and can well predict the experimental values of the Young's modulus, the Poisson's ratio, uniaxial compressive strength and others.

4.2 Sensitivity Analysis

Synthetic model is developed by using PFC^{2D}. Dimension of the bonded particle model, radius ratio, disk thickness, stress and element density are the same for all the runs performed during simulation.

Sensitivity studies define the dependency of geometrical and mechanical micro-properties (ball stiffness, contact stiffness, ball friction coefficient, ball radius., etc) on the overall set of macro-mechanical properties of the sample (Young's modulus E, Poisson ratio *v*, peak strength, cohesion C and friction angle ϕ). Contact normal strength and contact shear strength are increased from their calibrated values separately. The values of strength (normal and shear strength) used in the model are 0.60 MPa, 0.70 MPa, 0.80 MPa, 0.90 MPa, 1 MPa, 5 MPa and 8 MPa while the other parameters remain constant. The same approach is performed for particle friction coefficient, particles stiffness and particle radius.

Sensitivity is used to determine how different values of an independent variable will impact a particular variable (macro-mechanical properties) under a given set of assumptions. The advantage of doing sensitivity analysis is the possibility of studying the impact of different parameters and to identify how these factors affect the mechanical behavior of the assembly. In order to investigate the effect of different micro-physical properties, several studies were performed.

4.2.1 Effect of particle radius.

Particle size is mainly defined according to the rock minerology and texture. The results show that by changing particles radius from 0.30 mm, 0.35 mm, 0.40 mm and 1.0 mm macro-mechanical properties are slightly affected. The small variation of this properties is explained due to the small variation used for analising the effect of particle radius.

However, the calibrated model is made of particles (disks 2D) that have a dimension of 0.35 mm.Therefore, the scope of this study was to investigate relevant changes in macro-mechanical properties when the radius of the particle is changed to common values for sandstone radius.

Potyondy and Cundall (2002) suggested that particle size could influence the tensile strength. They established a relationship between particle size and fracture toughness by applying upon the sample a series of Brazilian test . The results showed a limitation in PFC

application when the tensile strength to compressive strength ratio is calculated. The problem relies in using unrealistic particle radius with the aim of obtaining the required values of strength ratio.

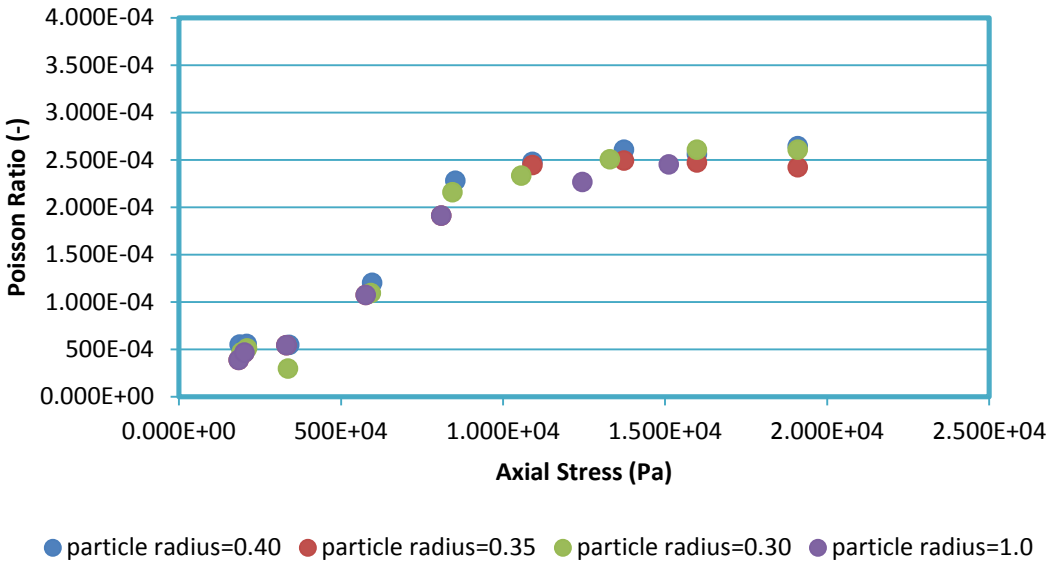

Fig.15: Poisson's ratio vs axial stress.

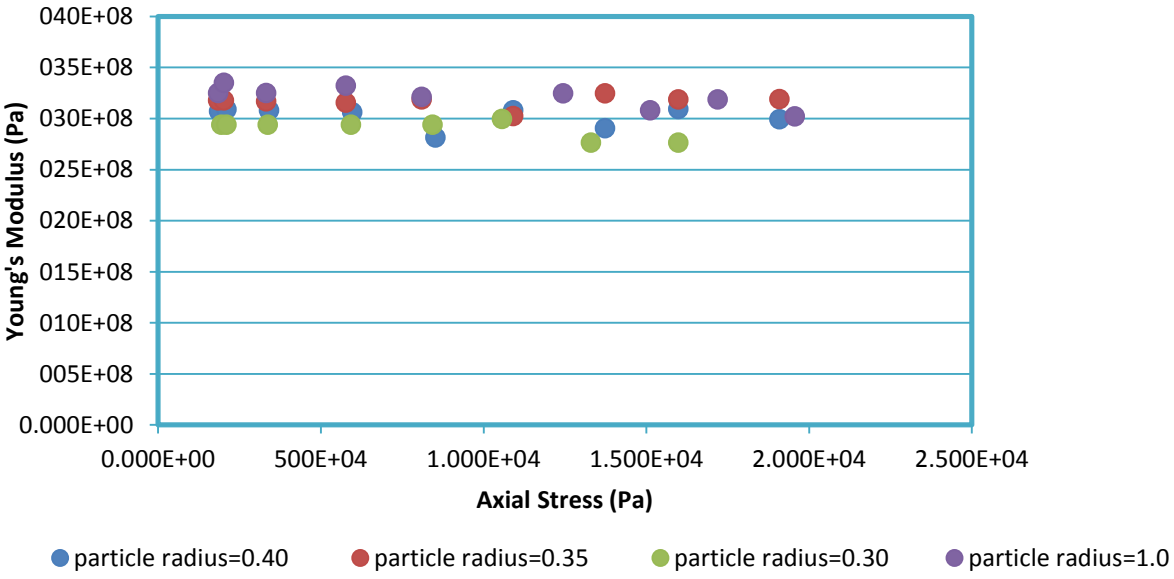

Fig.16: Young's modulus vs axial stress.

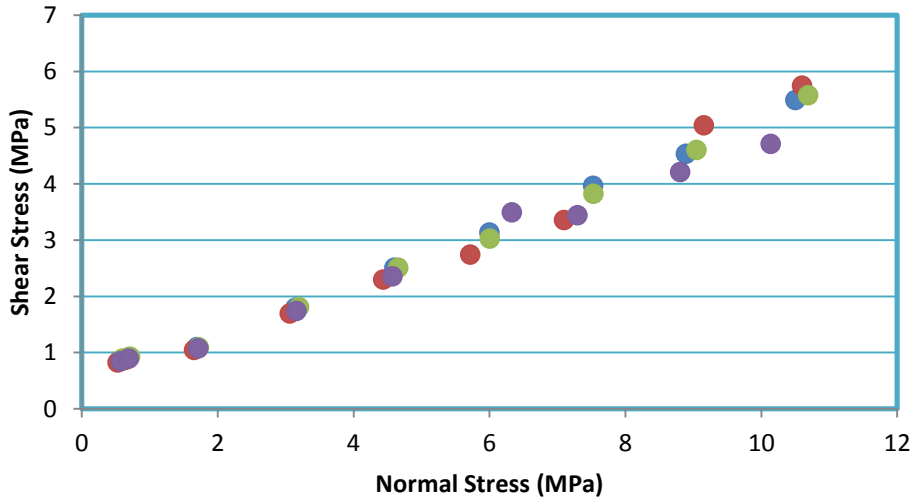

Fig.17: Mohr-Coulomb failure criterion.

Material stiffness shows slight variations from the Young's modulus obtained during the calibration process, when it is subjected to different particle radius dimensions.

The same behavior is observed during the estimation of Poisson's ratio. However, the variation found at the beginning of the analysis corresponds to the type of selected assembly. The type of bond selected in order to hold the particles together is contact bond.An assembly made of contact bonds instead of parallel bonds results (section 2) less constrains and therefore, Poisson's ratio values are far from the original values at the beginning of each experiment. Nevertheless, the values are quite stable (Poisson's ratio) during different case studies.

In case of failure criterion analysis, the calculations are performed by considering the axial and confined stress applied to the assembly. The analysis starts with axial stress σ1 and confined stress σ2. In an alternate version of Mohr-Coulomb failure criteria (σ1-σ2 space), a friction angle is estimated. This calculation allows estimating the failure parameters in σ-τ space that help to create the complete mechanical characterization of the assembly. Cohesion and friction angle are determined at different values of particle radius.

The increase of the particle radius results a little decrease of friction angle. Also, the tensile strength values show a small variation during simulations. As expected, the cohesive strength did not exhibit considerable changes at different particle radius. According to several studies cohesion is considered to be a function of parallel bond or contact bond normal and shear strength.

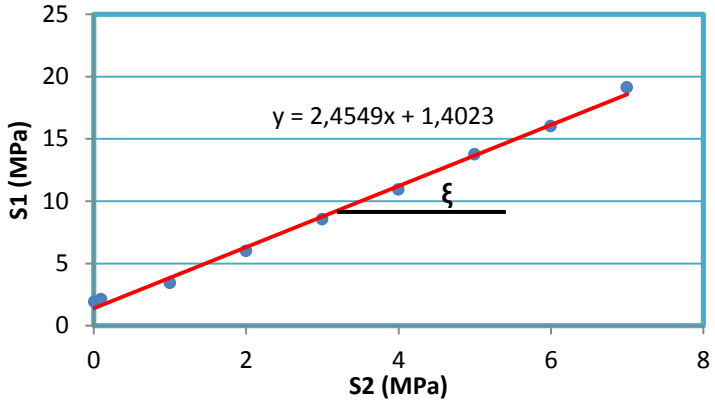

Fig.18: Alternate verion of Mohr-Coulomb failure criterion at R=0.40.

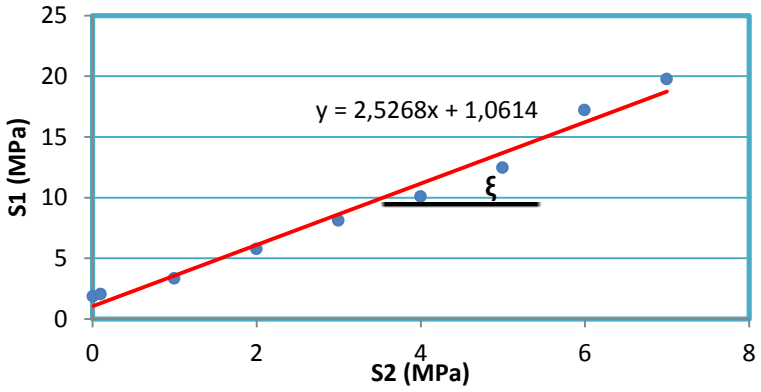

.

Fig.19: Alternate verion of Mohr-Coulomb failure criterion at R=0.35.

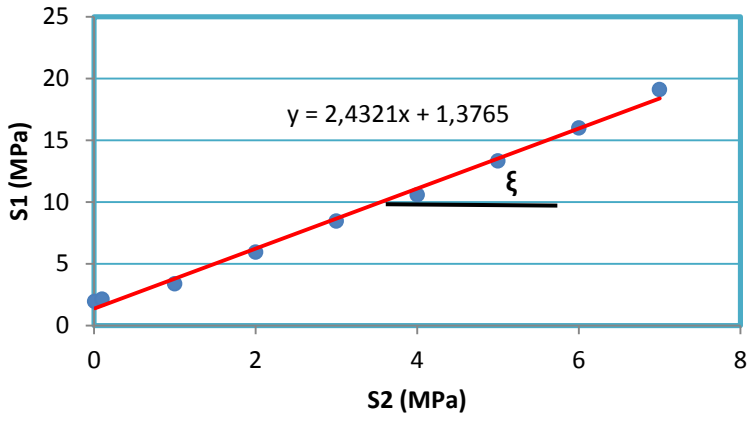

Fig.20: Alternate verion of Mohr-Coulomb failure criterion at R=0.30.

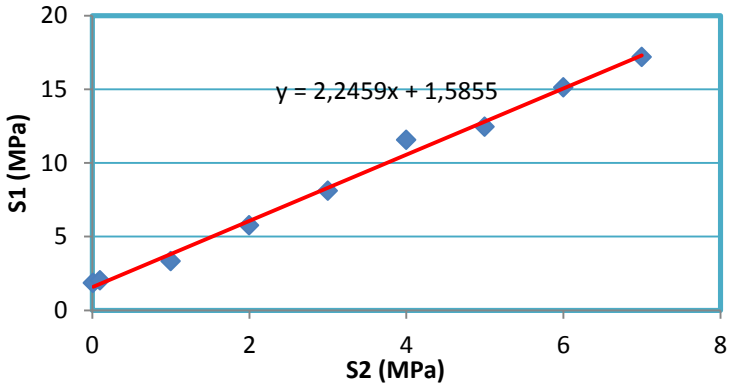

Fig.21: Alternate verion of Mohr-Coulomb failure criterion at R=1.0.

Case of Study	tan(ξ)	Friction Angle
R=0.40	2,4549	24,904
R=0.35	2,5476	25,864
R=0.30	2,4321	24,662
R=1.0	2,2459	22,571

Table.5: Sensitivity analysis results at different scenarios of particle radius while the others parameters remain constant.

The results obtained from different case studies show an internal friction angle around 24 to 25 degrees. Several analysis have pointed out that hard materials tend to break in shear at an angle of about 60 degrees (45 + φ/2). Therefore, 30 degrees is consideredas a good estimation for the angle of internal friction of many rocks. However, this values may vary greatly according to the type of rock (10 degrees for soft rocks and 50 degrees for hard rock).

4.2.2 Effect of particle friction coefficient

The effect of changing particle friction coefficient is observed over Poisson's ratio and Mohr-Coulomb failure criteria. The shear contact force ($F_s < \mu F_n$) at particle contact increases with the increase of friction coefficent and as a result, sliding between particles decreases. Nevertheless, the macro-failure criteria is dramatically affected by large change in friction coeffiecient.

At the beginig the sample is tested with small variation in friction coefficient (trial step 0.2). The macro-cohesion value and slope of the curve were slightly affected during the test. As a final point of experimentation the coefficient increases drastically. The case study where friction coefficient is increased up to 5.0 exhibits a clear influence over Poisson' ratio behavior due to the increase in particles strength and therefore the increase in material. The results are illustrated in Figure 24.

The cohesion of the material remains constant over different case studies even though internal friction angle changes during simulation. This results show similarities with the studies performed by T.Kazerani and J. Zhao (2008). Their investigation was based on Discrete Element Models and the effects of changing physical and mechanical properties of discretized models.

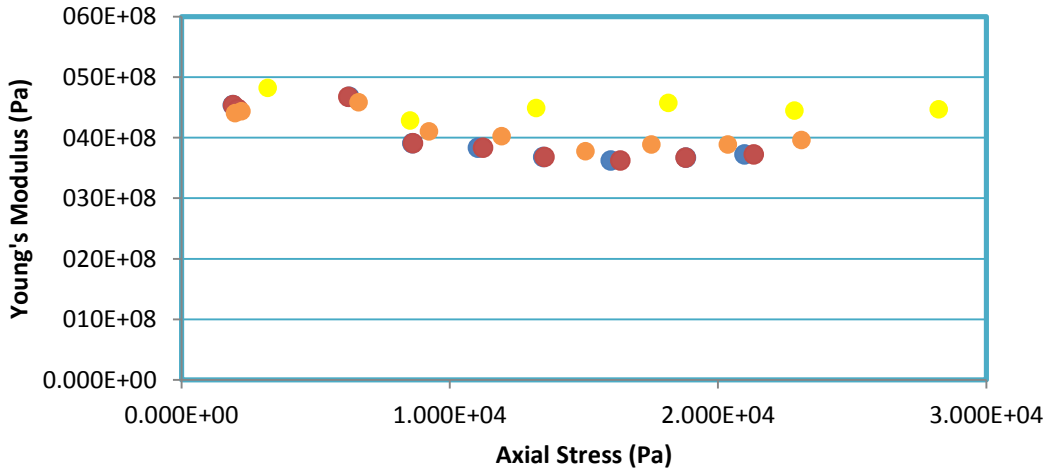

Fig.22: Young's modulus vs axial stress.

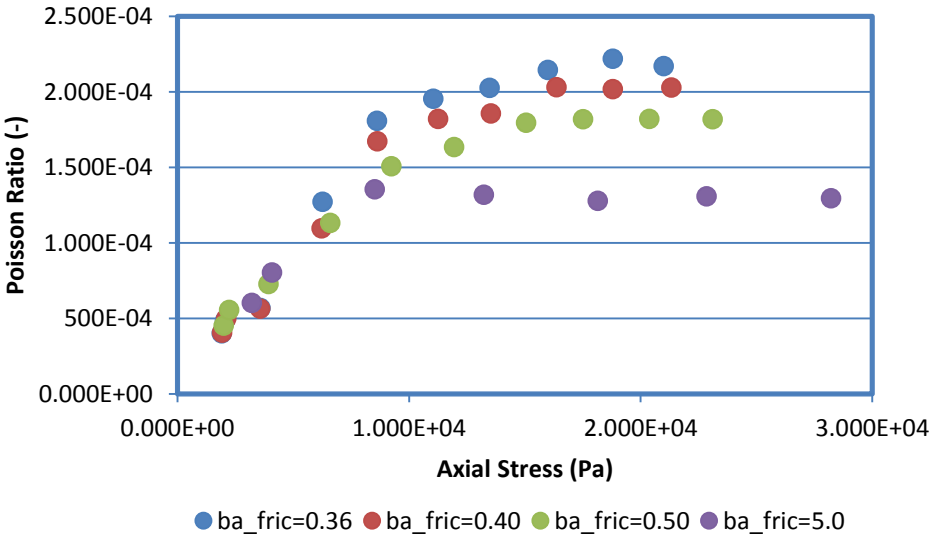

Fig.23 : Poisson's ratio vs axial stress.

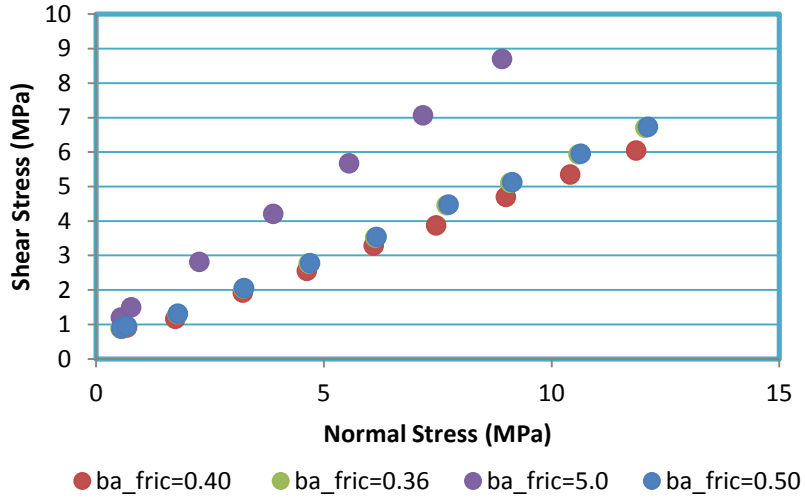

Fig.24 : Mohr-Coulomb failure criterion.

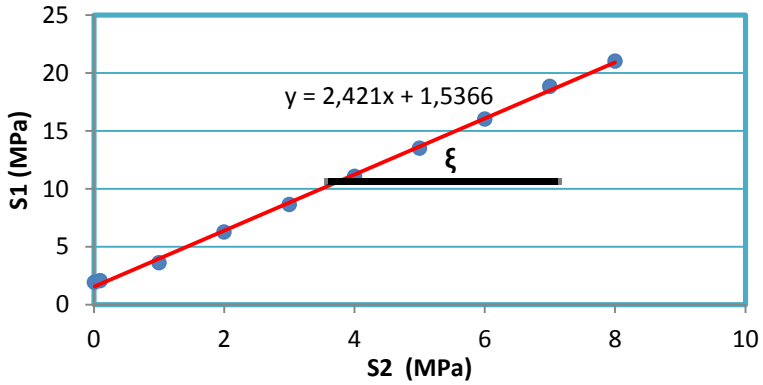

Fig.25: Alternate verion of Mohr-Coulomb failure criterion at friction coefficient 0.36.

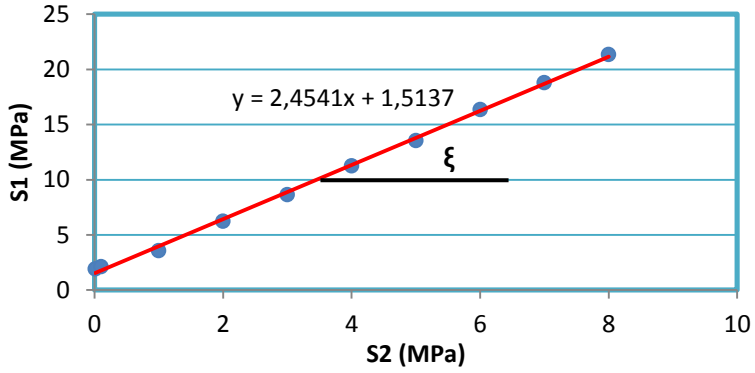

Fig.26: Alternate verion of Mohr-Coulomb failure criterion at friction coefficient 0.40.

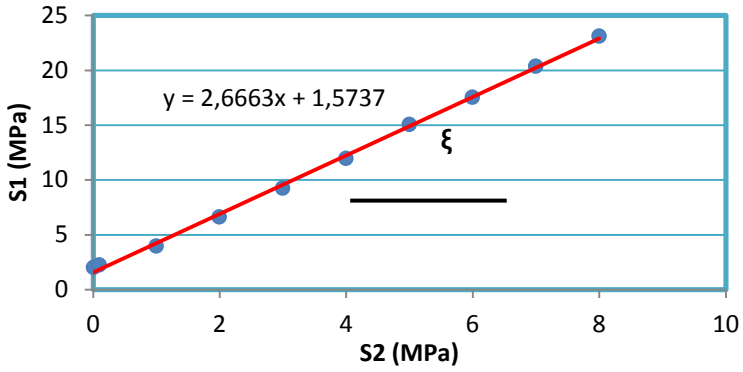

Fig.27: Alternate verion of Mohr-Coulomb failure criterion at friction coefficient 0.50.

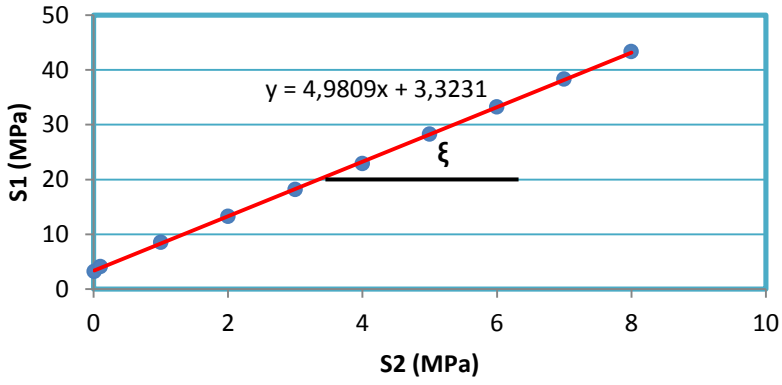

Fig.28: Alternate verion of Mohr-Coulomb failure criterion at friction coefficient 5.0.

Case of Study	tan(ξ)	Friction Angle
Friction coeff. = 0.36	2,421	24,547
Friction coeff. = 0.40	2,4541	24,893
Friction coeff. = 0.50	2,6663	27,032
Friction coeff. = 5.0	4,9809	41,728

Table.6: Sensitivity analysis results at different scenarios of particle radius while the others parameters remain constant.

4.2.3 Effect of normal contact stiffness

The figures 30, 31 and 32 show the response of the macro-mechanical properties of the assembly when normal contact stiffness is changed from 0.5E6 Pa to 1.0E2 Pa while the other parameters remain constant. Material stiffness and Poisson's ratio did not show any relevant variation during each case study. Mohr-Coulomb failure criterion exhibits as the same tendency as the previous analyzed variables (E and *v*).

Cohesion and friction angle of the model can be considered almost constant even though the strength of the contact has been decreased four orders of magnitude during simulation. This allows understanding the influence of contact bond strength over the macro-mechanical properties of the assembly.

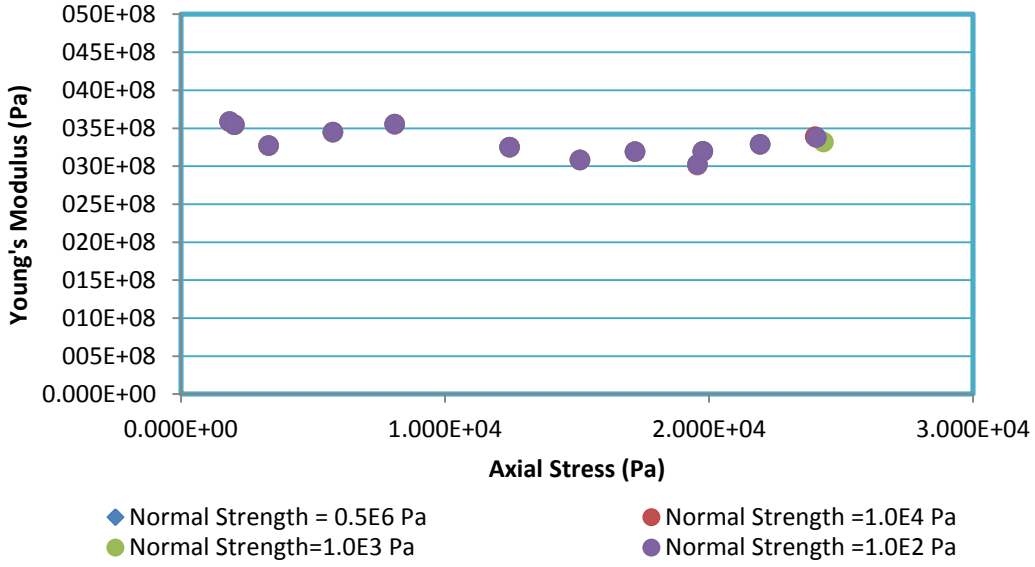

Fig.29: Young's modulus vs axial stress.

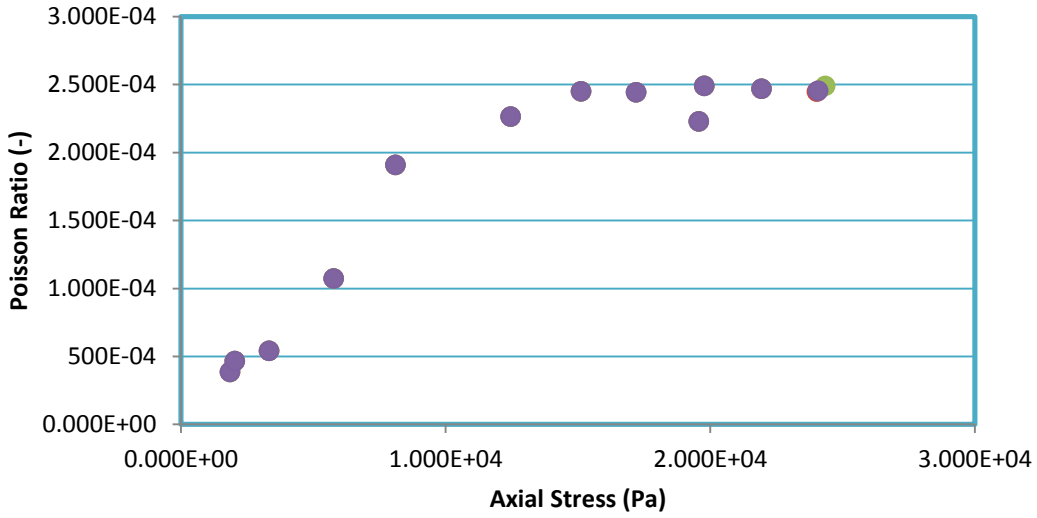

Fig.30: Poisson's ratio vs axial stress.

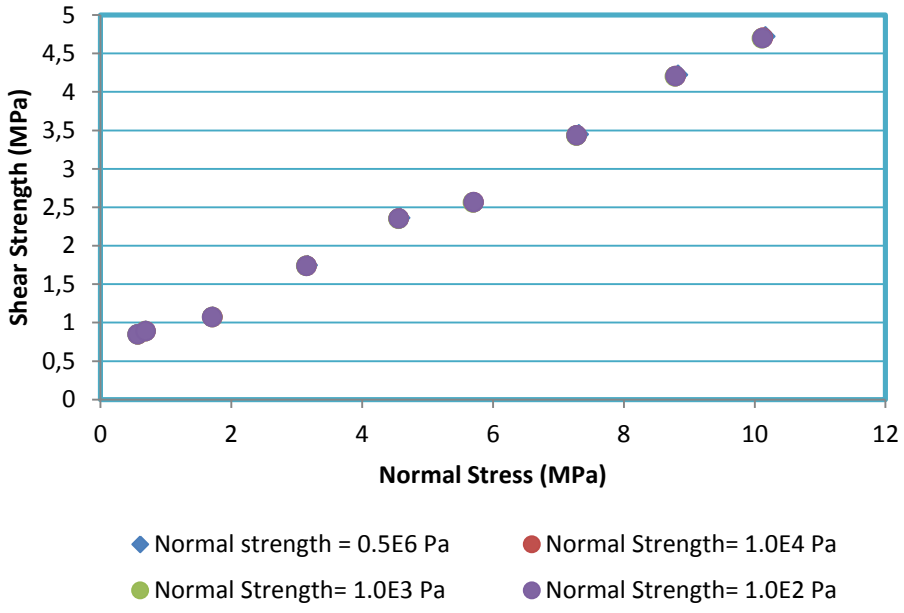

Fig.31: Mohr-Coulomb failure criterion.

Case of Study	tan(ξ)	Friction Angle
Contact Normal Strength = 0.5E6 Pa	2,2217	22,284
Contact Normal Strength = 1.0E4 Pa	2,2644	22,788
Contact Normal Strength = 1.0E3 Pa	2,2773	22,938
Contact Normal Strength = 1.0E2 Pa	2,2666	22,814

Table.7: Sensitivity analysis results at different scenarios of contact normal strength while the others parameters remain constant.

4.3 Fluid flow modeling evaluation.

Table 16 points out the values for fluid flow simulation. The mechanical properties were previously determined during the calibration process. The pressure is applied orthogonal to vertical axes, the injected fluid is water and it is assumed a 2D pipe network within the bonded particle model.

SRM PROPERTIES	International System Units (SI)
Hydraulic Aperture (ap_zero)	0.5
Permeability(k)	1.0E-8
Multiplier Factor (m)	0
Residual Fore (Fo)	1.0E10
Water Bulk Modulus (bulk_w)	2.2E9
Dynvisc_w	5.0E-4

Table.8: Fluid Flow Conditions within SRM.

A pressure range of 1 MPa to 0 MPa is distributed along the assembly from left to right respectively. Fracture aperture *a* is kept constant by considering a high value of contact normal compressive force (Fo >>> F) so there are any change in apertures within the model. The interaction between fluid and particles is not introduced at this stage of the simulation, in other words, there is no mechanical coupling. The main idea relies in modeling fluid flow through the pipes in order to monitor flow rate and permeability values at different points of the simulation until the system reaches steady-state conditions.

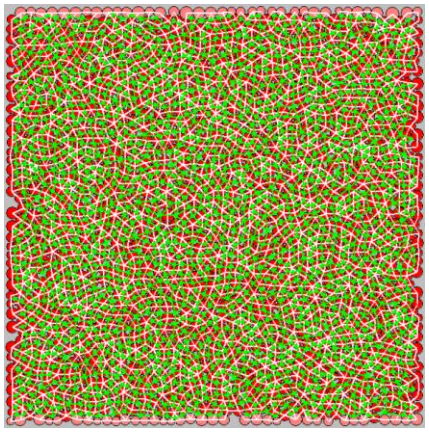

Fig.32: Bonded Particle Model and domains network.

The evolution of pore pressure after injection is presented in Figure XX. The pressure at domains starts to propagate along x-axis after 1 MPa of pressure is established at the left side of the bonded assembly. Pore pressure evolution is represented by green circles. The dimension of those circles is related to pressure values at each step of the simulation. At the beginning, the high pressure is located at the left side of the block but at the end of the simulation (23270 steps) the pressure distribution within the sample becomes uniform.

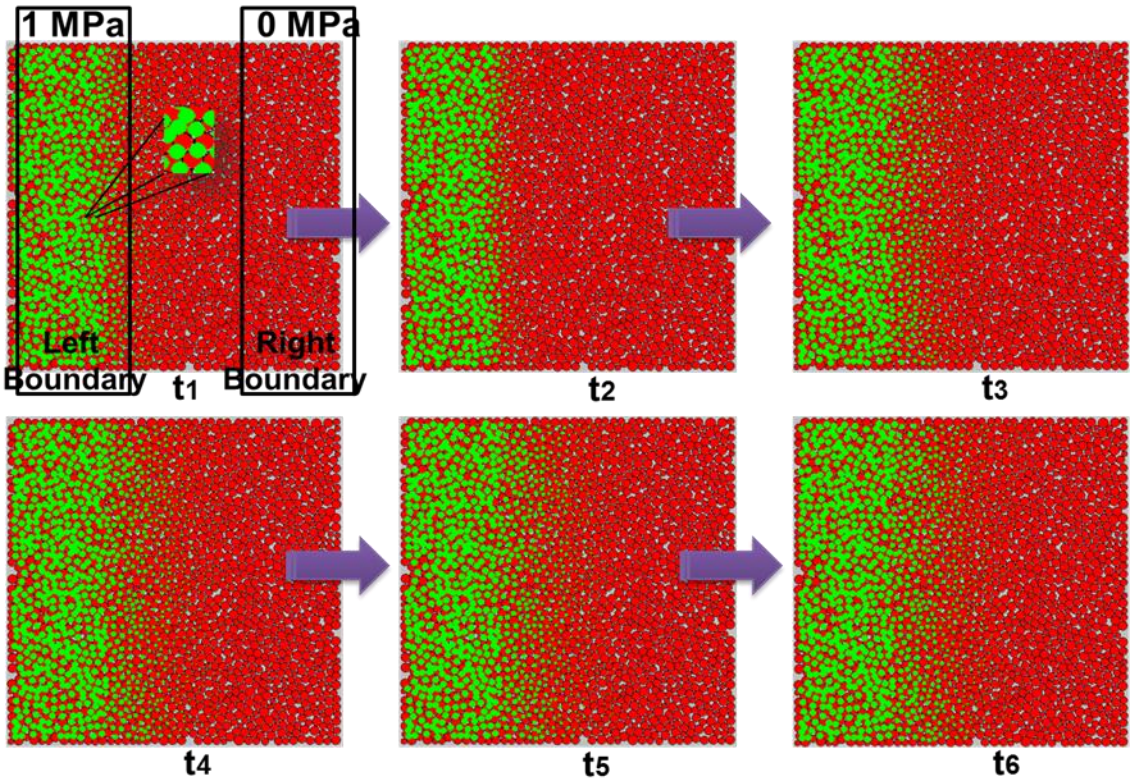

Fig.33: Pore pressure propagation along x-axis from left to right (pressure- green circles and bonded particles-red circles).

The development of tension and compression forces within the assembly is observed in Figure 35. Black lines represent compression forces while yellow lines show tension forces at contact points. As a result of pressure propagation through the defined domains, body forces due to the change of pore pressure are generated and therefore, the tension force increases. Initially, the higher tensile and compressive forces are located at the left side and before the system reaches steady-state conditions an increase in contact force is visible as a result of changing pore pressure along the sample.

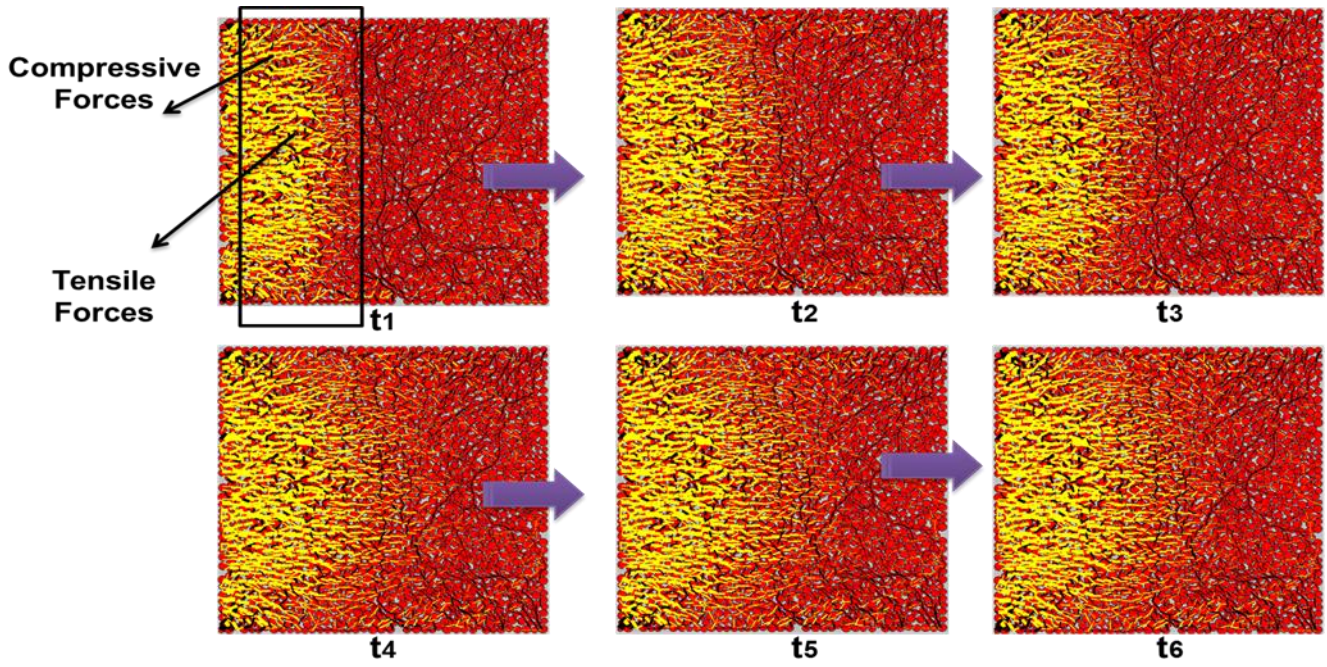

Fig.34: Evolution of tensile forces and compressive forces during fluid flow at contact points.

Permeability values are calculated at each step of the simulation by applying Darcy's equation. The calculated values exhibit an increasing tendency during transitory flow for finally reaches a stable value (constant permeability) that indicates uniform flow through the pipes. Parameters like viscosity, pipe length, cross sectional area and flow rate are introduced within the equation (Darcy's equation). Flow rate is calculated according to the amount of fluid going out of the sample (right side) and then dividing the volume by the flowing time. After flow rate is defined, Darcy equation is applied at the right boundary of the assembly and thus, permeability values are estimated at each step until the system is under steady state conditions.

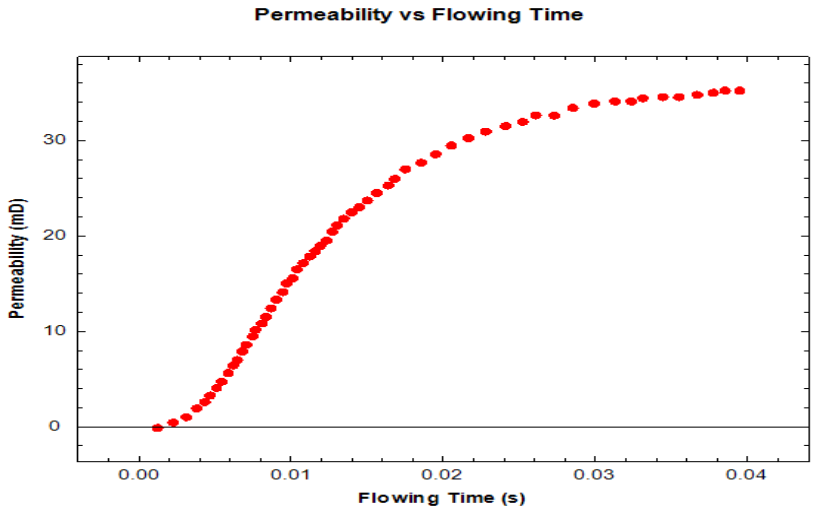

Fig.35: Permeability vs. flowing time calculated at right side of the sample.

Figure 37 represents the change in pressure within domains when a differential pressure of 1 MPa is applied to the bonded model. The y-axis corresponds to the pressure values within the fluid flow network while the x-axis represents the width of the sample. The plotted curves indicate the evolution of pore pressure along the horizontal dimension of the sample at different flowing time.

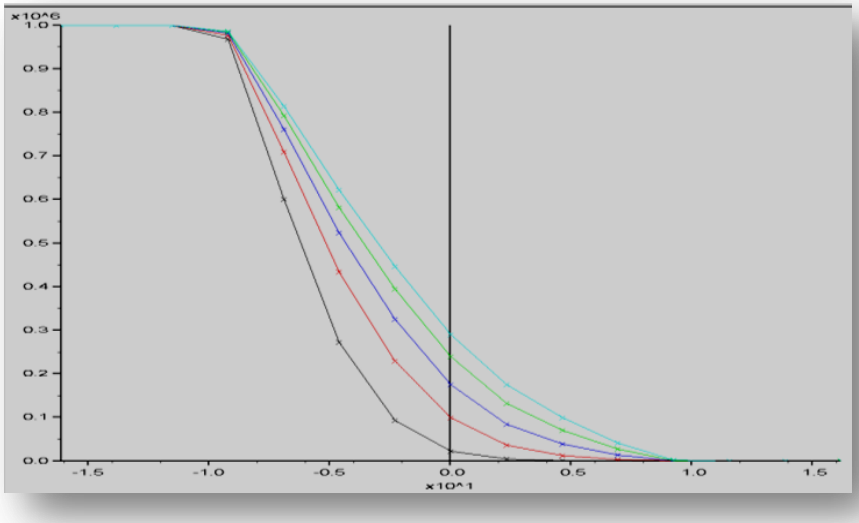

Fig.36: Pore pressure profile vs. sample dimension along x-axes at different flowing time.

4.4 Hydraulic fracturing modeling

Numerical simulation for hydraulic fracturing is done by injecting the fluid in the already made assembly having fluid network in it. The model has dimensions of 36 x 36 m having minimum particle size of 0.35 mm. the assembly was bounded axially and then vertical stress is imposed along the vertical axis. The injection point for the fluid is set to be at the center of the assembly and when the injection is started the first response of the assembly was hydraulic fracture. This is because the porosity of the assembly is low and the pressure distribution is slower then the mechanical forces exceeding the strength parameters of the assembly.

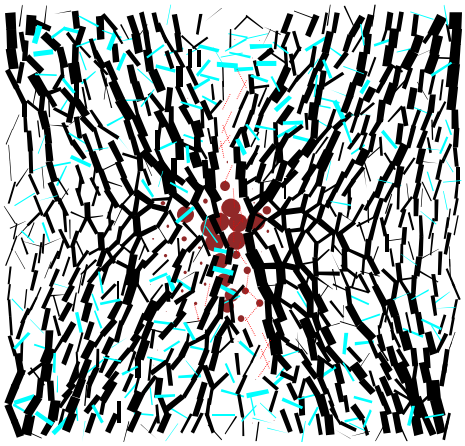

Fig.37: Compressive forces (black line), tensile forces (blue lines), bond opening (red lines) and injected fluid (brown-circles).

The fracture initiates at the injection point and propagate perpendicular to minimum stress direction. This agrees with the natural behavior of the rocks as fractures in rocks also opens along the axis where they have minimum resistance or minimum stress. In the simulated assembly the horizontal stress was lower than the vertical stress and as it is obvious from the simulated result the fracture propagated, as it should have in nature. The tensile fracture occurs because the mechanical forces exceed the tensile strength of the assembly. In the figure above the blue lines are tensile forces and black are the compressive

forces. The tensile forces are causing the fracture to propagate and open in this particular direction.

These results show that in PFC2D there is no need for pre-defining the point of fracture initiation and also the propagation direction. The assembly will decide the point depending on the forces in all the assembly and the bounding forces as well where the fracture should initialize and which direction it should propagate.

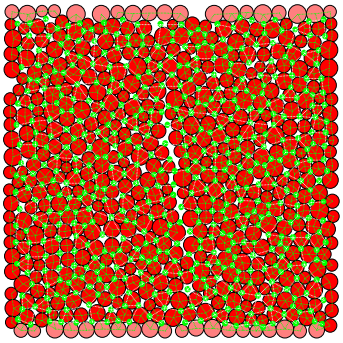

Fig.38: Fluid flow network (green dots), bonded particle (red disks) and bond opening due to fluid injection

5 CONCLUSIONS

A bonded particle model is created to simulate the injection of fluid through a hard rock. Synthetic Rock Mass (SRM) properties are calibrated with the aim of mimic rock properties prior disturbance (injection). PFC^{2D} is a useful tool for estimating fracture initiation and fracture propagation. The results obtained show:

- Good agreement with typical petrophysical and mechanical values of real sandstones.
- The performed sensitivity analysis shows the influence of changing different geometrical or physical parameters over sample macro-mechanical properties (particle size, particle friction coefficient, stiffness ratio, particle stiffness etc.).

Fluid flow simulation was performed within the rock mass by defining a fluid flow network made of parallel plate channels (located at each contact bond) and domains. The flow rate within each pipe and the stored pressure at domain center are updated during fluid calculation. There is no mechanical coupling during this simulation. The aim was to reproduce Darcy flow when the system reaches steady state conditions. In the beginning, pressure profile exhibits a transient flow with changing values in pressure and velocity during simulation. Subsequently, steady state conditions are obtained. Permeability value was consistent with characteristic value for low porosity sandstone.

Hydraulic fracturing represents the last step of study. The calibrated assembly is brought to an anisotropic state of stress. The load is distributed in a manner that the higher stress within the bonded particle material is in the vertical direction. A pressure of 1 MPa is injected at the center of the material. The strength of the contact bond adjacent to the injection area is overcome and therefore, a fracture is generated within the material. The fracture propagates in the direction with less resistance to opening (horizontal direction).The mode of fracture is mode I by opening of the SRM. The results of this simulation show the capacity of the software to reproduce hydro-fracturing at high pressures.

APENDIX

PARTICLE RADIUS=0.40			
S1 (MPa)	S2 (MPa)	τ(MPa)	σ(MPa)
1,88057	0,01	0,84831156	0,55142522
2,10068	0,1	0,90731701	0,67908478
3,41383	1	1,09468232	1,69866856
5,9667	2	1,79891556	3,14813743
8,52955	3	2,50767477	4,60049495
10,9095	4	3,13348805	5,99991317
13,7365	5	3,96204043	7,52872731
15,9918	6	4,53132439	8,89206634
19,0996	7	5,48722078	10,5021564

Table.9 : Sensitivity analysis results at particle radius R=0.40 while the others parameters remain constant.

PARTICLE RADIUS=0.35			
S1(MPa)	S2 (MPa)	τ(MPa)	σ(MPa)
1,84597	0,01	0,8260314	0,52752452
2,02656	0,1	0,86678924	0,6430601
3,32423	1	1,04570715	1,6551556
5,76768	2	1,6951377	3,06203631
8,10276	3	2,29581092	4,4383696
10,09	4	2,73998551	5,71665351
12,4515	5	3,35254549	7,1004341
17,1996	6	5,03887385	9,15695118
19,7734	7	5,74695089	10,600575

Table.10: Sensitivity analysis results at particle radius R=0.35 while the others parameters remain constant.

PARTICLE RADIUS=0.30			
S1(MPa)	S2(MPa)	τ(MPa)	σ(MPa)
1,94304	0,01	0,89008411	0,59980899
2,10773	0,1	0,92447574	0,7125984
3,37082	1	1,0916635	1,72338439
5,93058	2	1,80986778	3,19929822
8,44088	3	2,5052978	4,66012083
10,5722	4	3,02622336	6,00530909
13,2992	5	3,82143467	7,53225117
15,9918	6	4,60080621	9,04869714
19,0996	7	5,57136	10,6918289

Table.11: Sensitivity analysis results at particle radius R=0.30 while the others parameters remain constant.

PARTICLE RADIUS=1.0			
s1 (MPa)	s2 (MPa)	τ(MPa)	σ(MPa)
1,85	0,01	0,848	0,57562741
2,03	0,1	0,889	0,69353646
3,32	1	1,07	1,71605102
5,77	2	1,74	3,16075049
8,10	3	2,36	4,57206322
1,16	4	3,49	6,33001633
1,25	5	3,44	7,2956653
1,51E	6	4,21	8,80942112
1,72E	7	4,71	10,1423026

Table.12: Sensitivity analysis results at particle radius R=1.0 while the others parameters remain constant.

DISK FRICTION COEFFICIENT = 0.36			
S2 (MPa)	S1 (MPa)	τ(MPa)	σ(MPa)
0,01	1,92342	0,86896028	0,56469442
0,1	2,0586	0,90998256	0,68088069
1	3,59312	1,165899	1,74424307
2	6,26415	1,91838231	3,22458528
3	8,61588	2,5538172	4,63021047
4	11,0527	3,28903895	6,09953389
5	13,4841	3,87255763	7,47201876
6	15,9997	4,70239141	9,00173707
7	18,8034	5,35058425	10,4155062
8	20,9942	6,04744144	11,8603399

Table.13: Sensitivity analysis results at disk friction coefficient = 0.36 while the others parameters remain constant.

DISK FRICTION COEFFICIENT= 0.40			
S2 (MPa)	S1 (MPa)	τ(MPa)	σ(MPa)
0,01	1,92597	0,88639115	0,55283883
0,1	2,10642	0,95067668	0,68220822
1	3,57069	1,30943125	1,80191474
2	6,22984	2,04988615	3,25538008
3	8,63091	2,77718465	4,70078826
4	11,252	3,53766364	6,16651665
5	13,5386	4,47945507	7,74328342
6	16,3683	5,12885736	9,14098683
7	18,7975	5,9554301	10,647192
8	21,334	6,73203169	12,1227941

Table.14: Sensitivity analysis results at disk friction coefficient = 0.40 while the others parameters remain constant.

DISK FRICTION COEFFICIENT = 0.50			
S2 (MPa)	S1 (MPa)	τ(MPa)	σ(MPa)
0,01	2,00021	0,88639115	0,55283883
0,1	2,23455	0,95067668	0,68220822
1	3,94006	1,30943125	1,80191474
2	6,6026	2,04988615	3,25538008
3	9,2356	2,77718465	4,70078826
4	11,9431	3,53766364	6,16651665
5	15,0577	4,47945507	7,74328342
6	17,5158	5,12885736	9,14098683
7	20,3717	5,9554301	10,647192
8	23,1154	6,73203169	12,1227941

Table.15: Sensitivity analysis results at disk friction coefficient = 0.50 while the others parameters remain constant.

DISK FRICTION COEFFICIENT= 5.0			
S2 (MPa)	S1 (MPa)	τ(MPa)	σ(MPa)
0,01	3,21588	0,87027124	0,56931599
0,1	4,08395	0,89082023	0,67252265
1	8,52345	1,17941578	1,75800058
2	13,2282	1,93944199	3,24646302
3	18,1582	2,55424258	4,64159018
4	22,852	3,20774422	6,06159018
5	28,2292	3,85878071	7,48000585
6	33,2	4,54811347	8,9230342
7	38,3	5,36848131	10,4502777
8	43,3	5,91008691	11,7983631

Table.16: Sensitivity analysis results at disk friction coefficient = 5.0 while the others parameters remain constant.

NOMENCLATURE

d_g	= Grain diameter
K_o	=Empirical factor
T	=Tortuosity
$\emptyset$	=Porosity
k	=Permeability
F	=Formation resistivity factor
r_{eff}	=Effective pore radius
D	=Fractal dimension
P_i	=Inlet pressure
P_o	=Outlet pressure
Q_x	=Volumetric flux
W	=Fracture width
μ	=Dynamic viscosity
u'	=Average velocity
τ	=Shear stress
c	=Inherent shear strength or cohesion
σ_n	=Normal stress
ϕ	=Failure angle
C_0	=Uniaxial compressive strength
m	=Empirical curve-fitting parameter
C_{of}	=Uniaxial compressive strength of the fractured rock
F^n	=Tensile forces
F^s	=Shear forces
e_{3jk}	=Permutation symbol
$M_3^{[\emptyset_1]}$	
$x_i^{[C]}$	=Interception point
$x_i^{[A]}$	=Geometric center of body A
U^n	=Normal displacement
$\dot{x}_i$	=Translational velocity
w_3	=Rotational velocity
$\ddot{x}_\iota^{(t)}$	=Translational acceleration
$\dot{w}_3$	=Rotational acceleration
ΔU^s	=Shear displacement
g_i	=Body force acceleration vector
$\dot{H}_i$	=Angular momentum
I_1	=Moments of inertia
F_0	=Contact normal compressive force
a	=Aperture
k_f	=Fluid bulk modulus
V_d	=Apparent volume of the domain
q	=Flow rate
bulk_w	=Water bulk modulus

S_H	=Horizontal Stress
Sv	=Vertical Stress
E	=Young's modulus
ν	=*Poisson's ratio*
ξ	
S1	=Axial Stress
S2	=Confined Stress

REFERENCES

Branko Damjanac, Ivan Gil, Matt Pierce and Marisela Sanchez: "A new approach to Hydraulic Fracturing Modeling in Naturally Fractured Reservoirs", ARMA 10-400, 2010.

Carman, P. C: "Fluid flow through a granular bed", Trans. Inst. Chem. Eng. London, 15:150-156, 1938.

Cundall, P.: "Fluid Flow Formulation for PFC2D". Itasca Consulting Group: Minneapolis, Minnesota, 2000.

Cundall, P.A., and Strack, O.D.L: "A Discrete Numerical Model for Granular Assemblies", Gèotechnique 29, No.1: 47-65, 1979.

E. Fjaer, R.M. Holt, P. Horsrud, A.M. Raaen and R. Risnes: "Petroleum related rock mechanics 2nd Edition", 419, 2008.

Hansgeorg Pape, Christoph Clauser and Joachin Iffland: "Variation of Permeability with Porosity in Sandstone Diagenesis Interpret with a Fractal Pore Space Model", Applied Geophysics Journal, 2000.

Hoek, E. and Brown: "Practical estimates of rock mass strength", International Journal of Rock Mechanics and Mining Sciences, Volume 34:1165-1186, 1998.

James F. Hazzard, R. Paul Young and Stephen J. Oates: "Numerical modeling of seismicity induced by fluid injection in a fractured reservoir", 2004.

Kozeny, J.: "Über kapillare Leitung des Wassers im Boden, (Ausfstieg, Versickerung und Anwendung auf die), *Sitzungsber. Akad. Wiss.* Ber. Math. Nat. (Abt. IIa), 136a: 271-306, 1927.

Pape, H., Clauser, C., and Iffland, J.: "Permeability Prediction Based on Frcatal Pore SpaceGeometry, 1999.

Melvin Friedman, Texas A. and amp; M University: “Porosity, Permeability and Rock Mechanics”, ARMA-76, 1976.

N. Cho, C.D Martin , D.C.Sego and R.Christiansson: “Modeling Dilation in Brittle Rocks”, ARMA/NARMS 04-483, 2004.

Pape, H., and Schopper, J. R.: “Relations between Physically Relevant Geometrical Properties of a Multifractal Porous System”. In Characterization of Porous Solids (Elsevier, Amsterdam), 1988.

Particle Flow Code (PFC), Version 4, Minneapolis, Itasca Consulting Group, 2004.

Potyondy, D. O., and P. A. Cundall: “A bonded Particle Model for Rock”, Int. J.Rock Mech. & Min. Sci., 1329-1364, 2004.

Potyondy, D. O., Cundall, P.A., and Lee, C: “Modeling rock using bonded assemblies of circular particles”, 1996.

Robert P. Chapuis and Michel Aubertin: “Predicting the coefficient of permeability of soils using the Kozeny-Carman equation”, EPM-RT-03, 2003.

S.R.Brown: “Surface rougness and the physical properties of fractures”, Rock Mechanics Contributions and Challenges, Hustrulid & Johnson, 1990.

Tsang C. F and Y. W Tsang: “Channel Model of flow through fractured media”, Water Resources, 1989.

T.Kazerani and J. Zhao: “Micromechanical parameters in bonded particle method for modelling of brittle material failure”,International Journal for Numerical and Analytical Methods in Geomechanics, Vol 34.No18: 1877-1895,2010.

T. Kazerani and J. Zhao: “A Bonded Particle Modeling Rock Material”, ARMS5,2008.
Teng-Fong Wong, Christian David and Wenlu Zhu: “The transition from brittle faulting to cataclastic flow in porous sandstones: Mechanical Deformation”, Journal of geophysical research, vol 102, No.B2:3009-3025, 1997.